6-1-2015

Computational modeling analysis of mitochondrial superoxide production under varying substrate conditions and upon inhibition of different segments of the electron transport chain.

Nikolai I. Markevich
Thomas Jefferson University

Jan B. Hoek
Thomas Jefferson University

HHS Public Access

Author manuscript

Biochim Biophys Acta. Author manuscript; available in PMC 2016 June 01.

Published in final edited form as:

Biochim Biophys Acta. 2015 ; 1847(0): 656–679. doi:10.1016/j.bbabio.2015.04.005.

Computational modeling analysis of mitochondrial superoxide production under varying substrate conditions and upon inhibition of different segments of the electron transport chain

Nikolai I. Markevich[1,2,*] and **Jan B. Hoek**[1]

[1]MitoCare Center for Mitochondrial Research, Department of Pathology, Anatomy, and Cell Biology, Thomas Jefferson University, Philadelphia, PA 19107, USA

[2]Institute of Theoretical and Experimental Biophysics, Russian Academy of Sciences, Pushchino, Moscow region 14290, Russia

1. Introduction

Accumulating evidence over the past decades has demonstrated that reactive oxygen species (ROS), such as superoxide, hydrogen peroxide and other reactive forms of oxygen, are critical mediators in a broad range of cellular signaling processes [1, 2]. However, their production must be carefully controlled as the oxidative stress associated with uncontrolled ROS formation can cause damage to proteins, lipid membranes and DNA. ROS-induced cell and tissue injury plays a role in a broad range of disease conditions, from cancer to ischemic cardiac injury and stroke to neurodegenerative diseases and other age-related degenerative conditions [2, 3]. Understanding how cells are protected against oxidative stress damage requires an understanding both of processes that contribute to ROS formation and of oxidative stress defense capacities and cellular repair mechanisms.

The mitochondrial electron transport chain is one of the major contributors to ROS formation in most cells. Early studies by Chance and coworkers [4] had demonstrated that mitochondria generate H_2O_2 at a rate that is dependent on the respiratory substrate and oxygen levels and is influenced by the respiratory state and the presence of inhibitors of the electron transport chain. Work by many investigators has since confirmed that Complexes I and III of the mitochondrial respiratory chain are major sources of reactive oxygen species (ROS) in the cell, primarily generated in the form of superoxide $(O_2^{\cdot-})$. However, in spite of intensive biochemical and biophysical studies of electron and proton transfer in different segments of the electron transport chain (for reviews, see [5–9]) numerous questions about the mechanisms of $O_2^{\cdot-}$ generation remain unresolved. One of these is the identification of

*Corresponding author. Present address for correspondence: Nikolai Markevich, Institute of Theoretical and Experimental Biophysics, Russian Academy of Sciences, 3 Institutskaya street, Pushchino, Moscow region 14290, Russia, markevich.nick@gmail.com, Phone: +7 9160983229.

sites of $O_2^{\cdot-}$ formation in Complex I. There is a consensus that reduced $FMNH^-$ is one site of O_2 reduction by Complex I [5]. However, experimental data on the rate of ROS production by Complex I in mitochondria mediating forward and reverse electron transport show that at least one more site of $O_2^{\cdot-}$ production in complex I should be considered in order to account for experimental observations (for review see [6]). The Q-binding site was suggested as a site of superoxide formation in Complex I [7, 9, 10].

Another key unresolved question concerns the mechanism of bifurcated oxidation of ubiquinol at the Q_O site of complex III, especially the initiation of movement of the reduced Rieske iron-sulfur protein (ISPH) from the Q_O site to cyt c_1 [11]. While the crystal structure of Complex III is well established, there is no consensus about the exact sequence of dissociation of ISPH from the Q_O site and transfer of the second electron to cyt b_L. Crofts and colleagues [8, 12] suggested that dissociation of the reduced ISPH from the Q_O site, with further transfer of the first electron to cyt c_1, occurs before transfer of the second electron from semiquinone to cyt b_L (early ISPH dissociation). Other authors [11, 13–16] proposed that ISPH dissociates from the Q_O site only after transfer of the second electron from semiquinone to cyt b_L and cyt b_H, i.e. after cyt b_H reduction (late ISPH dissociation), which may be an important mechanism to protect Complex III from short-circuiting when both electrons transfer from QH_2 into the high potential c-chain. For a more detailed discussion of the arguments supporting one or the other hypothesis see [8, 11–13].

In addition, many questions related to ROS production upon inhibition of different segments of the respiratory chain remain unresolved. For instance, Brand and coworkers [17] showed recently that their experimental data on the rate of superoxide production by the antimycin-inhibited Complex III can be accounted for only by the assumption that the rate constants of ubiquinol oxidation at the Qo site are very low if cyt b_L is in the reduced state, which implies a complex dependence of binding QH_2 and Q to the Qo site on the redox state of cyt b_L. Another interesting feature first observed by Drose and Brandt [18] in submitochondrial particles and purified cytochrome *bc*1 complex from bovine heart mitochondria is the non-monotonic dependence of ROS production by antimycin-inhibited Complex III on the activity of succinate dehydrogenase and the concentration of the oxidized ubiquinone Q. In order to account for an unexpected decrease in ROS production by antimycin-inhibited Complex III with increasing the QH_2/Q ratio (an increase in ROS production with increasing oxidized ubiquinone Q) Drose and Brandt [18] proposed that oxidized ubiquinone supports ubisemiquinone formation and, respectively, superoxide production at the Qo site due to transfer of electrons from reduced cytochrome b_L onto Q in a reverse reaction of the Qo site. Later, this hypothesis was confirmed and studied in more detail experimentally in isolated mitochondria from skeletal muscle and with the help of a computational model by Brand and coworkers [17], who showed non-monotonic dependencies of ROS production by antimycin-inhibited Complex III on the concentration of different respiratory substrates for Complexes I and III and the reduced cyt b_L. These experimental and computational modeling results show that reverse reactions at the Qo site can play an important role in ROS formation by antimycin-inhibited Complex III and should be taken into account in studies of ROS production by the entire electron transport chain (ETC) with and without inhibitors of different segments of ETC.

Such questions are not unexpected for a system as complex as the respiratory chain, the analysis of which is difficult when based just on experimental studies. A computational systems biology approach can be helpful in these analyses, the starting point for which is a detailed computational model of the entire respiratory chain. Such a computational mechanistic model of electron transfer and superoxide formation in the mitochondrial respiratory chain, through which different hypotheses can be evaluated, is developed in the present study. In contrast to the rule-based model of the respiratory chain [19, 20], we applied a standard kinetic approach used previously for computational modeling of Complex III and the entire ETC [21–26] with an explicit presentation of the most important pathways of electron transfer in Complexes I and III. Besides, in order to explore possible differences in responses of ROS production in models taking into account the hypotheses mentioned above, pathways of electron transfer and superoxide formation in Complexes I and III were considered in more detail compared to other segments of the ETC . The model was analyzed under different conditions (forward and reverse electron transport, with and without different inhibitors of Complexes I and III) to account for available experimental data on ROS production, discriminate between different hypotheses and make predictions to be tested experimentally.

2. Methods and Models

2.1. Kinetic model of mitochondrial respiratory chain

A kinetic scheme of electron transfer and superoxide anion $O_2^{\cdot-}$ production underlying a mechanistic computational model of the mitochondrial respiratory chain is presented in Fig. 1, modified from a preliminary scheme presented in [27]. This simplified kinetic scheme includes the following electron carriers: a) for Complex I (NADH dehydrogenase, also known as NADH:Ubiquinone Oxidoreductase): flavine mononucleotide (FMN), the sequence of iron-sulfur clusters beginning with N3 and N1a and ending with the N2 cluster, and coenzyme Q; b) for Complex III (Cytochrome bc1 complex, also known as Ubiquinol:Cytochrome c Oxidoreductase): coenzyme Q, non-heme iron-sulfur protein (ISP), cytochromes b_L, b_H and c_1; c) Cytochrome *c*, and d) Complex IV (Cytochrome *c* oxidase). Complex II (Succinate dehydrogenase) and Complex IV are included as unresolved complexes, since these are not generally considered to be direct sources of ROS during mitochondrial electron transport. Electron transfer in Complexes I and III is described in detail in order to take into account the electron carrier states responsible for bypass reduction of O_2 resulting in $O_2^{\cdot-}$ formation. These bypass reactions are marked in red in the kinetic scheme (Figs. 1–2). The entire reaction network of electron transfer and superoxide production corresponding to this kinetic scheme in Fig. 1 consists of 40 reactions, the rate constants of which are described in detail in Table 1.

2.1.1. Kinetic model of Complex I—The initial steps of electron transfer in Complex I (reactions (1–5)) were taken from the kinetic model developed by Kussmaul and Hirst [28] for isolated Complex I. These authors proposed that $O_2^{\cdot-}$ is formed by the transfer of one electron from the fully reduced flavin $FMNH^-$ to O_2 (reaction (16) in Fig. 1 and Table 1). A detailed analysis of NADH/NAD^+ binding to Complex I is reviewed by Vinogradov [29]. Some kinetic constants of NADH oxidation coupled to the reduction of molecular oxygen

were assessed at the suggestion of a ping-pong mechanism [30]. More recently, it was shown that the kinetics of NADH oxidation and ubiquinone (Q) reduction in Complex I may not obey the classical ordered or ping-pong mechanism due to a strong spatial separation of these reactions and the presence of a buffer zone consisting of a chain of Fe-S redox centers between NADH- and Q-binding sites [31]. Moreover, using a fitting procedure, the authors [31] estimated rate constants of Q (QH_2) and NADH (NAD^+) binding to Complex I, as well as of electron tunneling between different redox centers, with the help of a stochastic model of Complex I, with the suggestion of a more complex mechanism taking into account the possible diffusion of quinone inside a broad ubiquinone binding pocket. In particular, within the framework of this model, the authors could account for an unusual experimental observation of substrate inhibition of Q reduction at high Q concentrations.

In the model presented here, for the kinetic description of electron transfer through the chain of Fe-S clusters we took into account the generally accepted suggestion that $FMNH^-$ donates the first electron to the Fe-S cluster N3 (reaction (6)). Electron transfer from N3 to the terminal cluster N2 through the chain of equipotential redox centers N1b, N4, N5, N6a, and N6b [5, 32] is approximated as a single step (reaction (7)) with an apparent rate constant of 10^4 s^{-1} since electron movement through the entire chain takes about 100 μs [33, 34]. Subsequently, the first electron transfers from N2 to oxidized ubiquinone Q bound to Complex I (reactions (8), (9)), reducing ubiquinone to semiquinone.

The second electron transfers from the semireduced flavin radical $FMNH^{\cdot}$ to either cluster N1a or cluster N3 (reactions (10) and (11)). Electron transfer from cluster N1a to cluster N3 is very slow ($k_{forward}$ is about of 160 s^{-1} [35]) compared to other reactions in Complex I. Therefore, we propose that cluster N1a only reversibly deposits single electrons without their delivery to the chain of seven redox centers. The kinetic model of electron transfer in the membrane domain of Complex I and the coupling mechanism of proton translocation through the membrane takes into account recent X-ray structures of complex I and the hypothesis of a “piston” mechanism of transmembrane H^+ movement, as reported by Sazanov and colleagues [36]. It is very likely, in accord with this mechanism, that 3 H^+ move through the mitochondrial membrane simultaneously (through transmembrane subunits NuoL, NuoM and NuoN) during electron transfer from N2 to quinone. We assume that a conformational switch and translocation of 3 H^+ occurs during electron transfer from reduced $N2^-$ to ubisemiquinone to form QH_2 (reaction (13)) reflecting the experimentally observed increase in ubisemiquinone concentration upon an increase in $\Delta\mu_{H+}$ [37, 38].

The path of the fourth proton translocation in Complex I is not clear [36]. It is very likely that the fourth proton transfer is also controlled by a conformational switch in the membrane arm [39]. The ROS production rate in Complex I and the redox state of flavin during oxidation of NAD-linked substrates don’t depend on the membrane potential in the presence of the quinone-binding site inhibitor rotenone [40, 41]. This implies that translocation of the fourth H^+ is also controlled by electron transfer from N2 to quinone or semiquinone in the quinone-binding pocket. We propose that the fourth H^+ translocation is also coupled with electron transfer from reduced $N2^-$ to semiquinone (reaction (13)). Therefore, we suggest that 4 H^+ move through the mitochondrial membrane simultaneously in reaction (13).

Reactions (8) and (14) in Fig.1 and Table 1 describe binding and dissociation of Q_n and QH_{2n}, respectively, in the quinone-binding site, where the subscript "n" refers to the negative side of the inner membrane.

Furthermore, we hypothesize that semiquinone in complex CI.$Q^{\bullet-}$ (Fig. 1 and Table 1) is the second site of $O_2^{\cdot-}$ formation in Complex I (reaction (17)). This hypothesis is supported by numerous lines of experimental evidence that ubisemiquinone can be one of the sites of superoxide generation in Complex I (for reviews see [6], [42]).

2.1.2. Kinetic model of Complex III—Fully reduced quinone QH_{2n} generated by Complex I or Complex II (reaction (19)) translocates to the positive side of the inner membrane (reaction (19)), and QH_{2p} is doubly oxidized at the Qo site of Complex III (reactions (22–26)). Then, oxidized Q_p is transported from the positive to the negative side of the inner membrane (reaction (20)), and Q_n is doubly reduced at the Qi site of Complex III (reactions (32–36)) completing Mitchell's Q-cycle [43] after binding and oxidation of the second QH_{2p} molecule at the Qo site.

The kinetic scheme of QH_{2p} oxidation at the Qo site presented in Fig. 1 is based mainly on the work of Crofts and colleagues [8, 12]. These authors suggested the initial formation of the ternary complex of cyt b_L, QH_{2p} and oxidized Rieske iron-sulfur protein, ISPox, (complex b_L.QH2.ISPox in Fig. 1) at the Qo site (reaction (22)) with the following bifurcated reaction where the first electron of QH_2 is transferred to the high-potential chain, consisting of ISP (reaction (23)) and cyt c_1 (reaction (27)). The second electron is transferred from the semiquinone $Q^{\cdot-}$ to the low-potential chain, consisting of cyt b_L (reaction (24)) and cyt b_H (reaction (25)). Electron transfer from the reduced Rieske iron-sulfur protein ISP (designated as ISPH in Fig. 1) occurs due to movement of the mobile extrinsic (or head) domain of ISP (ISP-ED) between the cyt *b* and c_1 positions that are defined as ISP-ED bound to the Q_O site and the ISP-ED position close to the c1 subunit, respectively [11, 44]. The states of ISP corresponding to a different position of the ISP-ED are designated in Figs. 1 and 2 as different complexes of ISPox and ISPH, where ISPox and ISPH mean the oxidized and reduced states of ISP-ED. The states of ISP with some intermediate position of ISP-ED between the b- and c1 sites are designated in Figs. 1 and 2 as free forms of ISPox and ISPH. Therefore, the description in the text of conformational changes in the states of ISPox or ISPH implies the domain movement of oxidized or reduced ISP-ED.

Crofts and colleagues [8, 12] proposed that ISPH moves from the b-position to the c_1-position (reaction (24)) before the second electron passes to cyt b_L. This is the basic kinetic scheme which relates to Tables 1 and 2. However, another hypothesis [11] suggests that the conformational switch of ISPH occurs only after the second electron transfers from cyt b_L to b_H. For comparison, the kinetic scheme of Complex III with the late ISPH dissociation is presented in Fig. 2A. The reaction network of electron transfer and superoxide production corresponding to this kinetic model of Complex III with the late ISPH dissociation (model L) consists also of 40 reactions, the rate constants of which are described in detail in Supplemental materials (Tables S1 and S2). In addition, we will consider the hypothesis proposed by Drose and Brandt [18] that oxidized coenzyme Q can leave the Qo site before

electron transfer from b_L to b_H occurs (reaction (41) in the modified kinetic scheme presented in Fig. 2B: b_L^-.Q.ISPH = b_L^-.ISPH+ Qp). This modified branched kinetic scheme of the Q-cycle takes into account the consecutive release of Q and ISPH from the Qo site and differs from the kinetic scheme presented in Fig. 2A by additional reactions (41), (42), (25a) and (34a). We will analyze all three hypotheses in the Results and Discussion section in order to reveal if one of these can account more effectively for available experimental data on ROS production.

Based on direct experimental observations [45] it is generally accepted that the unstable semiquinone of the Qo site (complex bL. $Q^{\cdot-}$) is the site of $O_2^{\cdot-}$ formation in Complex III. This $O_2^{\cdot-}$ is released to the IMS and matrix (reactions (28), (29)) [46]. The mechanism of separation of $O_2^{\cdot-}$ fluxes to these compartments at the Qo site is unclear. For the sake of simplicity, we assumed that the rate constants of $O_2^{\cdot-}$ release into the IMS and matrix are equal.

It should be pointed out, that in the development of the kinetic models of Complex III presented in Fig. 1, 2 we combined some experimentally observed individual reactions in one overall reaction, for instance, reactions (22) and (23) in all models and additionally reaction (26) in the model in Fig. 2A. The main reason for this was to reduce the number of model parameters, e.g. the rate constants of the individual reactions comprising a single reaction, absolute values of which are known only very approximately, and thereby exclude the intermediate states of these reactions that, in our opinion, are not critical for the analysis of ROS production (i.e., reaction (22) in all models and reaction (26) in the model of Fig. 2A). We understand that this simplification may result in some deviation of modeling the dependency of ROS production on different factors from that observed experimentally. Especially, this relates to the first electron transfer in reaction (23), which occurs according to a proton-first-then-electron mechanism [12]. This mechanism implies an initial formation of protonated semiquinone QH at the Qo site that can also participate in superoxide production. However, little is known about the p*K* values of QH [12], which is needed for a more detailed modeling of the first electron transfer. We believe that, taken together these simplifications in the models of Complex III may affect the computational modeling results on ROS production quantitatively, but not qualitatively. However, a more detailed consideration of some of these reactions, especially the first electron transfer, will be needed for a more exact quantitative description of the dependency of ROS production on these different factors.

2.2. Computational models of electron transfer in mitochondrial respiratory chain

Computational models consisting of 32 ordinary differential equations (ODEs) for the kinetic models presented in Figs. 1 and 2A and 34 ODEs for the branched model in Fig. 2B, plus 12 moiety conservation equations, were derived from the reaction networks using the law of mass action, Michaelis (more exactly: Henri-Michaelis-Menten [47]) and Hill equations for all 40 (44 for the branched model) kinetic processes. All equations are presented in Supplemental materials. The models were implemented in DBSolve Optimum software available at website **http://insysbio.ru** . The details of the mathematical model describing oxidized and reduced states of different carriers and electron flows through

Complexes I, II, III and IV are presented in Supplementary materials. Values of model parameters, rate constants and concentration of different electron carriers were taken from experimental data in the literature on thermodynamics and kinetics of electron transfer in the respiratory chain (Tables 1 and 2 and Supplemental Tables S1–S4).

Dimension of local and whole mitochondrial concentrations and rates— Experimental data on intramembrane protein concentrations presented in Table 2 are usually presented in nmole/mg mitochondrial protein, whereas we use concentration units (μM) in our computational model. Moreover, we use in the model local concentrations of proteins in different compartments of mitochondria, normalized by the relative volume fractions of these compartments. Therefore, NADH and matrix superoxide concentrations were normalized by the matrix water volume (V_{MX}), cyt *c* and superoxide concentrations in the intermembrane space (IMS) were normalized by the IMS water volume (V_{IMS}), and concentrations of all intramembrane proteins of the respiratory chain were normalized by the inner membrane volume (V_{IMB}). First, we normalized the concentration of all proteins by the total mitochondrial volume, V_{MIT}; then, total mitochondrial concentrations were translated into local concentrations using the water space fraction of matrix ($W_{MX}=V_{MX}/V_{MIT}$) and IMS ($W_{IMS}=V_{IMS}/V_{MIT}$), and the fractional volume ratio of inner membrane ($W_{IMB}=V_{IMB}/V_{MIT}$) to the total mitochondrial volume. In order to calculate W_{MX}, W_{IMS} and the total mitochondrial water space fraction, $W_{MITW}=V_{MITW}/V_{MIT}$, where V_{MITW} is the total mitochondrial water volume, we used the following experimental data. The mitochondrial water weight fraction, m_w/m_{mit}, where m_w and m_{mit} is the mass of mitochondrial water and mitochondria, respectively, equals 0.664 g/g wet weight for a total mitochondrial density, ρ_{mit}, ($\rho_{mit}=m_{mit}/V_{MIT}$) of 1.09 g/ml [48]. Because $m_w = \rho_w \cdot V_{MITW}$ and $m_{mit} = \rho_{mit} \cdot V_{MIT}$, where the water densities, ρ_w, and ρ_{mit} are 1 and 1.09 g/ml, respectively, we can calculate the total mitochondrial water space fraction, W_{MITW}. Since $m_w/m_{mit} = \rho_w \cdot V_{MITW} / \rho_{mit} \cdot V_{MIT} = W_{MITW} \cdot 1$ g/ml/1.09 g/ml =0.664 g/g, the total mitochondrial water space fraction, W_{MITW}, equals $0.664 \cdot 1.09=0.724$.

Taking into account that $W_{IMS} \approx 1/14 \approx 0.07$ of the total mitochondrial water space for the orthodox configuration [49], the matrix water space fraction $W_{MX} = W_{MITW} - W_{IMS} = 0.652$. These values of W_{IMS} and W_{MX} are in agreement with those used in [50]. The value of W_{IMB} was calculated as follows: The volume and inner membrane surface area of an average rat liver mitochondrion are 0.27 μm^3 and 6.47 μm^2, respectively [51]. Assuming an average inner membrane thickness of about 0.01 μm, $V_{IMB}=6.47\ \mu m^2 \cdot 0.01\ \mu m = 0.0647\ \mu m^3$ and the inner membrane space fraction ($W_{IMB}=V_{IMB}/V_{MIT}$) of a mitochondrion is approximately 0.24.

The mitochondrial protein weight fraction W_{wprot} is about 0.25 g/g wet weight [48], i.e., 1 mg mitochondrial protein corresponds to 4 mg mitochondrial wet weight and occupies 4mg/ 1090 mg/ml = 3.67·μl. Therefore, a mitochondrial content of any metabolite of 1 nmol/mg mitochondrial protein, when normalized to total mitochondrial volume, is equal to a concentration of 10^{-9} mole/ $3.67 \cdot 10^{-6}$ 1 = 273 μM, i.e. 1 μM = 3.67 pmol/mg mitochondrial protein.

In order to obtain local concentration of different proteins in the matrix, IMS and inner membrane, the total mitochondrial concentrations were divided by their volume fractions, W_{MX}, W_{IMS} and W_{IMB}, respectively. Thus, total local intramembrane concentrations of ubiquinone (Q) and Complexes I and III had the following values: total Q = 4 nmol/ mg mit prot = 4541 μM; ISP = cyt b_L = cyt b_H = cyt c_1=0.325 nmol/ mg mit prot = 369 μM; FMN=N3=N1a=N2=0.2 nmol/ mg mit prot = 227 μM.

In order to present computer simulated rates of respiration and ROS production, which occur only in the inner membrane, in units of whole mitochondrial rates we multiplied all the rates of intramembrane processes by W_{IMB} = 0.24. In addition, in order to compare computer simulated rates of respiration and ROS production presented in the current paper in μM/s with experimentally observed rates expressed in pmol/min/mg protein the computer simulated rates can be multiplied by a factor of 3.67*60 = 220, i.e. 1 μM/s = 220 pmol/min/mg mitochondrial protein.

3. Results and Discussion

3.1. ΔΨ and ΔpH dependency of the ROS production rate with different respiratory substrates

ΔΨ dependency—Experimental observations show that the rate of ROS generation by Complexes I and III depends on the respiratory substrates that serve as fuel for Complexes I and III (for review see [6]). As a rule, the ROS production rate is low when only NADH-linked substrates are available, and this rate can be augmented by rotenone. A much higher ROS production rate by Complex I is observed in the presence of succinate alone, due to reverse electron transport, which is diminished by rotenone. Combined use of succinate and NAD-linked substrates results in an increase in the ROS production rate compared to NADH alone and a decrease in ROS production compared to succinate alone. In general, the rate of ROS production under different conditions changes as follows: (succinate + rotenone) < NADH alone < NADH + rotenone < NADH + succinate < succinate alone < succinate + Antimycin A. However, some experimental observations show that these relationships can change. For instance, in rat brain mitochondria ROS production in the presence of succinate alone is less than with NADH + rotenone [52, 53], in bovine heart submitochondrial particles, succinate alone and NADH + succinate are less than NADH + rotenone [54]. One of the reasons for these differences may be the very high sensitivity of the ROS production rate to changes in membrane potential ΔΨ observed experimentally [55–57] and theoretically with the help of a simplified computational model of ETC [23].

Our computational modeling results confirm the high ΔΨ sensitivity of the ROS production rate and predict that the relationships mentioned above when using different respiratory substrates can change due to changes in ΔΨ. Fig. 3 presents the computer simulated steady state ΔΨ dependency of the ROS production rate at different sites of Complex I (Fig. 3A, B) and Complex III (Fig. 3C) as well as for the entire respiratory chain (Fig. 3D). These findings are in essential agreement with recently published modeling results for cardiac mitochondria [23] and experimental data on ΔΨ dependency of ROS production by isolated mitochondria during oxidation of succinate alone [57] and NADH-linked substrates [55] and by isolated Complex III (cytochrome bc_1 complex) reconstituted into phospholipid vesicles

[56]. For example, the computer simulated dependence of the total superoxide generation rate on membrane potential during oxidation of NADH alone presented in Fig. 3D is very close qualitatively and quantitatively to the experimentally observed ΔΨ dependency of the rate of H_2O_2 production during oxidation of glutamate + malate or α-ketoglutarate in isolated brain mitochondria (Fig. 1 in [55]). The experimentally observed approximate values of 95 ± 5 and 40 ± 5 pmol/min mg prot. at ΔΨ equal to 180 and 160 mV, respectively, in the presence of glutamate + malate (Fig.1 in [55]) are close to computer simulated values of 0.4 and 0.15 μM/s corresponding to 88 and 33 pmol/min mg prot., respectively, at ΔΨ equal to 180 and 160 mV in NADH-supported superoxide production in Fig. 3D (note that a ROS production rate of 1 μM/s equals 220 pmol/min/ mg prot). These computer simulated results are also quantitatively close to experimental data on the total ROS production rate in liver mitochondria using different respiratory substrates in the presence and absence of rotenone [58, 59]. For example, the succinate supported ROS production rate in isolated liver mitochondria is about of 200 pmol/min mg prot with succinate alone and 3 pmol/min mg prot in the presence of rotenone [58], which is close to the computer simulated approximate values of 0.9 and 0.02 μM/s in the presence of succinate alone and succinate + rotenone (Fig. 3D), which corresponds to 198 and 4.4 pmol/min mg prot. Moreover, Figs. 3D and 3A show that the ROS production rate by Complex I during NADH oxidation becomes independent of ΔΨ in the presence of rotenone, compatible with experimental observations that uncoupler doesn't affect ROS generation in the presence of rotenone [40, 41]. This result reflects the fact that the ΔΨ-dependent step (reaction (13)) of electron transfer in Complex I is inhibited by rotenone. In our computer simulations we had to take into account a second site of superoxide production in Complex I, namely the ubisemiquinone radical (complex CI.$Q^{\cdot-}$ in Fig. 1), which generates $O_2^{\cdot-}$ during reverse electron transport at very high membrane potential (Fig. 3B). This observation is compatible with experimental data on ROS production in mitochondria from skeletal muscle during oxidation of succinate [7]. Elimination of this site for consideration of ROS formation would result in neglecting the ROS generation rate in the presence of succinate alone, as presented in Fig. 3A (only the $FMNH^-$ site would participate in superoxide formation in this case), which contradicts experimental observations [7].

Fig. 3E and F present the dependence of the respiration rate on ΔΨ and the relationship between the rates of respiration and total ROS production by the entire respiratory chain when using different respiratory substrates. The maximal respiration rate during NADH + succinate oxidation is approximately equal to the sum of the maximal respiration rates for oxidation of NADH alone and succinate alone, at least at low membrane potentials (Fig. 3E), whereas the total ROS production rate is maximal during oxidation of succinate alone (Fig. 3D). These results show that the ratio of the rates of respiration and ROS production are highly dependent on ΔΨ as well as on the nature of the respiratory substrates (Fig. 3F) and can vary over a range of 0.1–1 % at the parameter values used in our base model (Tables 1 and 2). These values are close to experimental data obtained with liver [58] or brain [53] mitochondria using different respiratory substrates, although they differ somewhat from the values of 1–2 % widely cited in the literature [60, 61]. Possible important reasons for the different values of the ratio of the rates of respiration and ROS production were reviewed by Murphy [62], who pointed out several factors which make extrapolation of ROS production

by isolated mitochondria to the *in vivo* situation invalid. The most important of these is that maximal ROS production occurs during RET, i.e. during oxidation of succinate alone. However, when glutamate/malate was used as physiological substrates H_2O_2 production was approximately 0.12% [53] of respiration. In addition, it should be pointed out that recent experimental and computational modeling studies [63] show that the net emission of hydrogen peroxide (H_2O_2) from mitochondria as well as the experimentally observed ratio of the rates of ROS production and respiration can strongly depend on the activity of glutathione/thioredoxin scavenging systems.

These computer simulated results were obtained in the model corresponding to the kinetic scheme presented in Fig. 1. It should be pointed out that different hypotheses on the movement of ISPH in complex III (early and late dissociation of ISPH from the Qo site as presented in Figs 1 and 2A) give results that are quantitatively very similar when using the same parameter values in the models.

Absolute values of the rates of ROS production by the mitochondrial ETC in different experimental studies are highly variable in different tissues and in the same tissues under different conditions (for review [2]). This applies to studies in forward and reverse electron transport as well as with and without different inhibitors of ETC. For instance, maximal values of the ROS production rate may vary from 130 pmol/min mg protein in human cortex mitochondria up to 2650 pmol/min mg protein in mitochondria from rat skeletal muscle when succinate alone was used as respiratory substrate and from 3 pmol/min mg prot. in rat liver mitochondria up to 174 pmol/min mg prot. in mitochondria from rat brain in the presence of succinate + rotenone (all data reproduced from Table 1 in [2]). Therefore, the main goal of this paper was primarily to present an analysis of possible qualitative features of ROS production with the different kinetic models presented in Figs. 1 and 2, rather than a quantitative description of ROS generation in a concrete experimental context. Relative changes in the rates of ROS production under variable conditions (different respiratory substrates and inhibitors of ETC) in the same experiments were more important for this study. Nevertheless, the values of kinetic parameters of superoxide production by different sites in our models were chosen such that the computer simulated rates of superoxide generation were close to those observed in liver mitochondria [58] [59].

ΔpH dependency—As pointed out by Lambert and Brand [57] the ROS production rate should depend equally on ΔpH and ΔΨ. However, their experimental studies unexpectedly show a much stronger sensitivity of ROS generation rate by Complex I to ΔpH than to ΔΨ in the presence of succinate alone [57]. Importantly, this feature is also observed in our computational model (Fig. 4A). The computational modeling analysis accounts for this phenomenon by the much stronger inhibition of the rate of electron transfer in Complex III with an increase in ΔpH than in ΔΨ. This is due to inhibition of the rate-limiting step of QH_2 oxidation in Complex III (reaction (23)) resulting from dissociation of H^+ into the intermembrane space in reaction (23). This results in a much slower rate of QH_2 oxidation in Complex III and a greater increase in QH_{2n} concentration with increasing ΔpH than ΔΨ (Fig. 4B). As a result, the excess of QH_{2n} forces additional reverse electron transfer in Complex I and increases the ROS production rate in this Complex. Computer simulation

shows (Fig. 4C) that this effect was attenuated when the analysis was carried out on the assumption that reaction (23) is independent of ΔpH and ΔΨ.

However, some experimental observations [58] show no difference in ΔpH and ΔΨ sensitivity of the ROS generation rate. Our computer simulation analysis accounts for these different experimental observations by the relationship of the rate limiting steps in the Qo and Qi site reactions of the Q-cycle. In other words, this depends on which of these sites, the Qi or Qo site, limits the rate of electron transfer in the Q-cycle. A 3-fold decrease (from 900 to 300 s^{-1}) in the rate constant of dissociation of QH_2 from the Qi site (reaction (36)) makes this step limiting in the Q-cycle and results in equal sensitivity of the ROS production rate to ΔpH and ΔΨ (Fig. 4D). Therefore, by inhibiting the Qo or Qi site we can control a difference in ΔpH and ΔΨ sensitivity of the ROS production rate. In summary, our computational model faithfully and quantitatively accounts for the characteristic features of ΔpH and ΔΨ dependence of ROS formation at different sites in the electron transport chain and provides a mechanistic underpinning for these observations.

3.2. Effects of inhibition of different segments of the respiratory chain on the ROS production rate

The ability of rotenone to increase ROS production by Complex I by inhibiting Q binding to complex I has been extensively studied experimentally (for review see [6]). Computer simulation results on stimulation of ROS production in the presence of rotenone (Fig. 3D) are quantitatively compatible both with published experimental observations that show a 3–10-fold increase in ROS generation by rotenone during oxidation of NADH-linked respiratory substrates [6] and computer simulated results for cardiac mitochondria [23]. In order to simulate the effect of rotenone, we suggested that $v_8 = v_{14} = 0$ in the computational model. Such a high stimulation of ROS production by rotenone is observed in our model in the range of membrane potential below approximately 160 mV during oxidation of NADH alone and with NADH+succinate (Fig. 3D).

In further analyses, in order to discriminate between computational models that derive from kinetic schemes with different mechanisms of QH_2 oxidation in the Qo site presented in Figures 1 and 2 (with early and late ISPH dissociation and involving oxidized quinone dissociation from reduced cyt b_L) the effects of different inhibitors of Complexes III and IV on ROS production were simulated.

3.2.1. Inhibition of the Qi site—Antimycin A (AA) is the most widely used inhibitor of the Qi site of complex III in experimental [64] and computational [23] studies of ROS generation in the respiratory chain because of its ability to enhance ROS production. AA binding to the Qi site near cyt b_H inhibits electron transfer from cyt b_H to ubiquinone at the Qi site. However, the exact mechanism of this inhibition is not clear, because a widely accepted hypothesis about competition between AA and Q for binding to the Qi site contradicts some experimental observations [65]. In order to simulate computationally the inhibitory effect of AA on the Qi site we applied the minimal hypothesis that AA inhibits completely the rate of electron transfer from cyt b_L to b_H at the Qi site (reaction (34)), i.e. $v_{34} = 0$ in the presence of AA. It should be noted that $v_{34}=0$ intrinsically results in

suppressing the reactions of electron transport from the semiquinone to cyt b_L and from cyt b_L to cyt b_H at the Qo site, i.e. $v_{24} = 0$ and $v_{25} = 0$ at steady state for the following reasons. First, inhibition of reaction (34) results in inhibition of all reactions of electron transfer at the Qi site at steady state, i.e. $v_{32} = v_{33} = v_{34} = v_{35} = v_{36} = 0$. Second, inhibition of the Qi site results in suppressing the reactions of electron transfer at the Qo site at steady state due to a break in the Q cycle. Because the concentration of reduced cyt b_H, $[b_H^-]$, and the complex of reduced cyt b_L with oxidized Q, $[b_L^-.Q]$, (see Fig. 1) are governed by differential equations $d[b_H^-]/dt = v_{25} - v_{32}$ and $d[b_L^-.Q]/dt = 2 \cdot v_{24} - v_{25} - v_{34}$ which equal 0 at steady state, therefore, $v_{25} = v_{32} = 0$ and $v_{24} = v_{25} = v_{34} = 0$ at steady state, i.e. $v_{24} = 0$ and $v_{25} = 0$. It should be noted that all these arguments are valid also for the model with late ISPH dissociation (Fig. 2A). (For detail see the mathematical models corresponding to different kinetic schemes in Supplementary data). A detailed analysis of the branched model in which oxidized Q can leave or bind to the Qo site when cyt b_L is reduced will be presented below in the section 3.2.5. The Q-dependence of ROS production by antimycin-inhibited Complex III.

Fig. 5 presents the computer simulated superoxide production rate by complexes I and III with succinate as respiratory substrate in the absence or presence of AA, for different computational models deriving from kinetic schemes presented in Figs 1 and 2A.

These computer simulation results predict that models with early (model E) and late (model L) ISPH dissociation will show different quantitative and qualitative responses in ROS production upon application of AA. Model L predicts (Fig. 5B, D) a very large increase in the rate of ROS production in the presence of AA with decreasing membrane potential, which is compatible with the experimentally observed [64] strong stimulation of H_2O_2 production in antimycin-supplemented rat and pigeon heart mitochondria by the addition of protonophores and ionophores. By contrast, model E (Fig. 5A, C) shows a non-monotonic profile and a decrease in AA-stimulated ROS formation at low membrane potential. These different computer simulated AA-induced ROS responses at low membrane potential in models E and L are accounted for as follows. The activity of cytochrome *c* oxidase (Complex IV) is very high at low membrane potential. Therefore, all electron carriers located downstream of the reaction blocked by AA, i.e., ISP, cyt c_1 and cyt *c*, become completely oxidized. The extremely low ISPH concentration at low membrane potential shifts the equilibrium of reaction (24) to complex $b_L^-.Q$ in model E (see for detail Supplementary Fig. S1). Therefore, the concentration of the $O_2^{\cdot-}$ producing site complex $b_L.Q^{\cdot-}.ISPH$ and the rate of ROS production by Complex III become negligible at low membrane potential in model E (Fig. 5A, C). By contrast, the concentration of the complex $b_L.Q^{\cdot-}.ISPH$ in model L does not depend directly on the concentration of ISPH. Therefore, a large decrease in the ISPH concentration upon depolarization of the mitochondrial membrane in the presence of AA should not strongly affect ROS production in model L. In order to clarify the mechanism of a large increase in ROS production by AA-inhibited Complex III observed in model L upon computer simulated depolarization (Fig. 5B, D), an analysis of ΔΨ-dependent reaction (23) in model L was carried out.

Our computational analysis shows that in model L an increase in ROS production by AA-inhibited Complex III upon depolarization occurs due to ΔΨ-dependent release of the first

H^+ of QH_2 into the intermembrane space (IMS) in the reaction (23) at the Qo site (Fig. 2A). Depolarization facilitates the release of H^+ into the IMS and shifts the equilibrium in this reaction toward formation of the unstable semiquinone, the complex $b_LQ^{\cdot-}$.ISPH. The efficacy of ΔΨ-dependent H^+ release depends on how readily H^+ diffuses through the membrane to the IMS after its release from the Qo site and is characterized by the dimensionless parameter δ1. If δ1 = 0 no increase is observed in the concentration of the unstable semiquinone in Complex III and the rate of ROS production by Complex III (Supplementary Fig. S2A and S2B) upon depolarization of the inner mitochondrial membrane. By contrast, the higher δ1, the more steeply ROS production increases upon depolarization (Fig.S2A and S2B). Experimental observations show that H_2O_2 production in AA-inhibited mitochondria can be stimulated as much as 13-fold by the addition of protonophores [64]. The steepness of the ΔΨ-dependency of ROS production in the presence of AA suggests the conclusion that δ1 may be considerable and will have to be taken into account in the modeling study. The suggestion that the second proton has to travel a considerable distance (after the first proton passes to ISPox) to go from the protonated semiquinone to the IMS aqueous phase is supported by molecular dynamics simulations and crystallographic studies of Complex III reviewed in [8]. These studies show that protonated semiquinone passes a proton to Glu-272 of cyt *b*, the side chain of which rotates so that the carboxylic acid group contacts a water chain leading to the IMS aqueous phase [8]. Thus, the second proton does appear to travel a large distance to reach the IMS aqueous phase after it leaves the semiquinone bound to the Qo site. We have used δ1 = 0.2 in our computational model.

It should be pointed out that our computations predict a decrease in the total ROS production rate in the presence of AA compared to the uninhibited condition at ΔΨ > 145 mV during oxidation of succinate alone in both models (Fig. 5A,B), even though an increase in the rate of $O_2^{\cdot-}$ generation by the unstable semiquinone of the Qo site of Complex III is observed over the entire range of membrane potential (Fig. 5C,D). The antimycin-induced decrease in the total rate of ROS production at ΔΨ>145 mV results from a strong decrease in the rate of $O_2^{\cdot-}$ generation by the semiquinone of Complex I upon inhibition of Complex III (data not shown). This effect will be considered in more detail below with inhibition of the Qo site of Complex III (Fig. 7C). In addition, our computations predict an increase in the total ROS production rate over the entire range of ΔΨ upon inhibition of the Qi site by AA during oxidation of NADH+succinate in both, E and L, models (Supplementary Fig.S2A and S2B). This occurs due to the strong increase in the rate of $O_2^{\cdot-}$ formation by $FMNH^-$ of Complex I upon inhibition of Complex III (Fig. 7B).

Of special interest is the ROS production rate upon partial inhibition of the Qi site by AA. Experimental studies show that the dependence of the rate of electron transport in uncoupled submitochondrial particles [66] and isolated bc_1 complexes [67] on the concentration of AA is sigmoid rather than linear. This means that a low concentration of AA has little inhibitory effect on the activity of electron transport at low membrane potential. Moreover, recent experimental [68] and theoretical [69] studies show that a low concentration of AA can stimulate the activity of isolated dimeric bc_1 complexes due to inter-monomeric electron transport between cytochrome *b* subunits. In the current study, we don't consider the

concentration dependency of AA, but analyze computationally the effect of AA-induced alterations in the rate of electron transfer from cyt b_L to b_H at the Qi site, i.e. the rate constant k_{34}, on the rates of respiration and ROS production. In order to take into account possible alterations in membrane potential upon a partial inhibition of the Qi site we analyzed changes in k_{34} at different $\Delta\Psi$.

Fig. 6 presents the analysis of the effect of a decrease in k_{34} on the rates of respiration (Fig. 6A) and ROS production (Fig. 6B–E) by different sites of the electron transport chain at different membrane potential values. As shown in Fig. 6A, the respiratory rate has a sigmoidal dependency on k_{34} and decreases very slowly when k_{34} decreases from 10^5 to 10–100 s^{-1} at different $\Delta\Psi$. This implies that reaction (34) limits the rate of electron transfer in the Q-cycle at values of $k_{34} < 100\ s^{-1}$. The same sigmoidal k_{34}-dependence is observed in the total rate of ROS generation by both Complexes I and III (Fig. 6B) and in the rates of ROS formation by the reduced flavin of Complex I (Fig. 6C), the unstable semiquinone of Complex III (Fig. 6D) and the semiquinone of Complex I (Fig. 6E). The rates of ROS production by different sites also slightly depend on k_{34} over the range above 10–100 s^{-1}, i.e. in a range of k_{34} where there is only a modest inhibition of the Qi site by AA. A transition of the respiratory rate from high to low levels when the Qi site is strongly inhibited by AA, (i.e. when k_{34} decreases below 10–100 s^{-1}), is accompanied by a transition to a high total rate of ROS production. The $\Delta\Psi$ dependency of ROS production at different sites also differs when AA inhibition of the Qi site is modest or strong. The effects of alterations in AA inhibition (reflected in k_{34}) and $\Delta\Psi$ on ROS formation at the reduced flavin of Complex I are presented in Fig. 6C. Both factors, a decrease in k_{34} and an increase in $\Delta\Psi$, reduce electron carriers of Complex I and thereby stimulate ROS production by the reduced flavin. The effect of either of these is most effective in the absence of the other factor. Hyperpolarization of the inner mitochondrial membrane strongly stimulates ROS production by $FMNH^-$ when the Qi site of Complex III is only weakly inhibited by AA (i.e. at high k_{34}), but does not affect ROS formation when AA -induced inhibition of Complex III is almost complete. By contrast, the rate of ROS generation by AA-inhibited Complex III at $k_{34} < 10\ s^{-1}$ is stimulated very strongly by depolarization of the inner mitochondrial membrane (Fig. 6D) as discussed above. However, a decrease in $\Delta\Psi$ inhibits ROS production by the unstable semiquinone when Complex III is only moderately inhibited by AA. As shown above (Fig. 3B) the rate of ROS production by the semiquinone of Complex I is negligible at $\Delta\Psi < 140$ mV in the absence of AA. Fig. 6E confirms this result and shows negligible ROS production at the $CI.Q^{\cdot-}$ site at $\Delta\Psi < 140$ mV with both partial and complete inhibition of Complex III by AA. However, the semiquinone of Complex I forms $O_2^{\cdot-}$ at a considerable rate at very high values of membrane potential ($\Delta\Psi = 180$ mV) and this rate is almost independent of inhibition of Complex III by AA, confirming that it is a direct effect of $\Delta\Psi$ on the four protons extruded through Complex I. Fig. 6F shows computer simulated relationships between the rates of respiration and overall ROS production by both Complexes I and III upon partial inhibition of the Qi site by AA at different $\Delta\Psi$. All curves represent data shown in Fig. 6A and 6B. An important feature of these relationships is the existence of a plateau in the dependence of ROS production on the respiratory rate. This means that the rate of ROS production by the AA-inhibited respiratory chain has a weak sensitivity to the rate of respiration and remains almost constant before the respiratory rate

reaches saturation. This feature differentiates ROS production in the electron transport chain without any inhibitors (see for comparison Fig. 3F) and upon partial inhibition by AA. This difference is accounted for by the fact that the main source of ROS is different in the presence and absence of AA. The main source of ROS in the AA-inhibited electron transport chain is Complex III (Fig. 6D) while sites of Complex I prevail in ROS formation in the absence of the inhibitor.

3.2.2. Inhibition of the Qo site—Stigmatellin and myxothiazol are well known inhibitors of the Qo site of Complex III which have different effects on the ROS production rate [55, 70–72]. X-ray crystallographic studies of complex III [44, 73] show that these inhibitors occupy the quinol binding pocket of the Qo site, so, they may compete with quinol for binding to the Qo site [12]. On the other hand, stigmatellin and myxothiazol bind to different domains of the quinol binding pocket (for reviews see [11, 12, 74]). Stigmatellin binds to the distal domain near the 2Fe2S cluster of ISP, so, stigmatellin fixes the extrinsic domain of ISP (ISP-ED) in the cythocrome b position while myxothiazol occupies the proximal domain close to the b_L heme and doesn't result in a fixed ISP-ED positioning [75].

Despite these achievements in understanding the structure-function relationships in Complex III, there is no a consensus on the exact steps of QH_2 oxidation in the Qo site that are inhibited by stigmatellin and myxothiazol. Differential effects of stigmatellin and myxothiazol on ROS production by Complex III could help clarify this situation. Experimental observations show [70] that isolated bc1 complexes generate $O_2^{\cdot-}$ in the presence of myxothiazol, while stigmatellin completely prevents ROS production by the bc1 complex. Moreover, myxothiazol stimulates ROS production in mitochondria, although less so than AA [70]. In order to clarify the underlying steps, we modeled the rate of ROS production in the respiratory chain with models E and L using a simulated response to inhibition of the first and second electron transfer in the Qo site. We assume the rate of reactions (23) and (24) to equal 0 in the presence of succinate as respiratory substrate (Fig. 7). It should be noted that models E and L show the same results for simulated ROS production rates when $v_{23}=0$ and $v_{24}=0$. Therefore, Fig. 7 presents results only for model E.

Inhibition of the first electron transfer in the Qo site ($v_{23}=0$): Fig.7 shows that inhibition of the first electron transfer ($v_{23}=0$) results in a large decrease in total ROS production rate (Fig. 7A) due to a strong inhibition of superoxide anion generation by the semiquinone of Complex I (Fig. 7C) and elimination of $O_2^{\cdot-}$ formation by the unstable semiquinone of the Qo site of Complex III (Fig. 7D). A large increase in the rate of $O_2^{\cdot-}$ formation by $FMNH^-$ of Complex I (Fig. 7B) when $v_{23}=0$ cannot compensate for the overall decrease in the ROS production rate. These computer simulated results are compatible with the experimentally observed effect of stigmatellin on the ROS production rate both in cytochrome bc1 complexes isolated from bovine heart and yeast [55, 71, 72] and in rat heart and brain mitochondria [70].

Inhibition of the second electron transfer in the Qo site ($v_{24}=0$): Computer simulated results of the ROS production rate upon inhibition of the second electron transfer in the Qo site ($v_{24}=0$) are also presented in Fig. 7. These results show that the ROS production rate

when v_{24}=0 is identical to the rate obtained under conditions that simulate the AA presence (v_{34} = 0) in model L (Fig. 5B, D). The total ROS production rate under these conditions is very high (much higher than in the uninhibited control) over the entire range of membrane potential below a ΔΨ of approximately 145 mV (Fig. 7A). This high total ROS production rate is accounted for by a very strong increase in the rate of $O_2^{\cdot-}$ formation by the unstable semiquinone of Complex III (Fig. 7D). A decrease in the total ROS production rate compared to the control at ΔΨ > 145 mV occurs due to a strong decrease in the rate of $O_2^{\cdot-}$ formation by semiquinone of Complex I (Fig. 7C). These computer simulated results are compatible with experimental observations that myxothiazol stimulates ROS production in brain [70] and liver [71] mitochondria although less so than AA. This observation can be accounted for as follows. Myxothiazol partly inhibits the first electron transfer due to its competitive inhibition of QH_2 binding to the Qo site. This results simultaneously in an activating (due to inhibition of the second electron transfer) and an inhibitory action on ROS production by Complex III (because of partial inhibition of the first electron transfer). Our computational data presented in Supplementary Fig. S3 confirm the hypothesis that simultaneous complete inhibition of the second electron transfer and partial inhibition of QH_2 binding to the Qo site by myxothiazol can account for the experimentally observed stimulation of ROS production, which is weaker than that obtained by AA [70].

It should be noted that the total ROS production rate increases over the entire range of ΔΨ upon inhibition of the second electron transfer in the Qo site during oxidation of NADH alone or NADH + succinate (Supplementary Fig. S4).

3.2.3. Inhibition of cytochrome c oxidase—Based on experimental observations of oxidative cellular injury during ischemia and reperfusion, which decreases cytochrome oxidase activity, some authors [76–78] proposed that inhibition of cytochrome c oxidase may facilitate ROS production by the respiratory chain. However, a direct experimental measure of ROS production in intact rat heart mitochondria and corresponding submitochondrial particles (SMP) [77] showed that an increase in ROS production upon inhibition of cytochrome *c* oxidase by azide was observed only in SMP oxidizing NADH.

In order to understand what changes in ROS production rates occur at different sites of the respiratory chain upon inhibition of cytochrome *c* oxidase, we used the computational modeling analysis, simulating inhibition of cytochrome *c* oxidase by assuming that the rate v_{40} = 0 in models E and L.

The computer simulated ROS production rate in model L with complete inhibition of cytochrome *c* oxidase (i.e., v_{40} = 0) with NADH as a respiratory substrate, is presented in Fig. 8. Fig. 8A shows that the simulated total ROS production by Complexes I and III significantly increases upon inhibition of cytochrome *c* oxidase compared to the uninhibited control at low membrane potential (ΔΨ < 120 mV), whereas practically no changes in ROS production occur at ΔΨ > 120 mV. This increased level in total ROS production is completely accounted for by a very strong increase in the rate of $O_2^{\cdot-}$ formation in Complex I at the $FMNH^-$ site, over the entire range of membrane potential (Fig. 8B). In this case, inhibition of cytochrome *c* oxidase results in identical changes in ROS production by Complex I as when Complex I is inhibited by rotenone (see Fig. 3A). A modest decrease in

the simulated rate of $O_2^{\cdot-}$ formation by the semiquinone of Complex I as well as by the unstable semiquinone of Complex III at $\Delta\Psi < 120$ mV is observed when $v_{40} = 0$ (Fig. 8C, D). However, ROS production by the unstable semiquinone of Complex III decreases considerably at $\Delta\Psi > 120$ mV.

It should be pointed out that curves related to NADH-induced superoxide production presented in Fig. 8 as well as above in Fig. 3 and below in Fig. 10 exhibit a notable dip, which indicate the possible existence of bistability (two alternative stable states in the rates of respiration and ROS production under otherwise identical conditions) in the operation of the respiratory chain. The phenomenon of bistability in ROS production by the mitochondrial electron transport chain was first observed experimentally by Selivanov and colleagues and accounted for with the help of their rule-based model [19, 20]. Bistability of Complex III was recently confirmed computationally in the six-state model with the native parameters [24]. A detailed analysis of this phenomenon in the entire respiratory chain was carried out by us with the help of an earlier version of our computational model and recently published elsewhere [27]. It was shown [19, 20] that during oxidation of any respiratory substrates, succinate or/and NADH-linked substrates, hysteresis and bistability in the entire respiratory chain can arise owing to the specific features of the Q-cycle in Complex III, in which the Qo and Qi site compete for the substrate ubiquinone reflecting total intramembrane ubiquinone conservation (for detail see [19, 20, 27]). The physiological implications of a possibility that the respiratory chain can exist in two alternative stable states with different rates of ROS generation is discussed in these earlier publications [19, 20, 27]. In particular, it was suggested [19, 20] that this phenomenon may be critical to account for the oxidative stress resulting from anoxia/re-oxygenation (ischemia/reperfusion). A detailed analysis of hysteresis and bistability in the respiratory chain is beyond the scope of this paper, therefore, we do not devote further attention to this phenomenon here.

Interestingly, in contrast to NADH oxidation, using succinate as a substrate for the respiratory chain results in the opposite results (Fig. 9), i.e., all computer simulated rates of ROS production decrease upon inhibition of cytochrome c oxidase ($v_{40} = 0$) compared to the condition without the inhibitor, including the total ROS production rate (Fig. 9A), the rate of $O_2^{\cdot-}$ formation by the semiquinone of Complex I (Fig. 9C) and by the unstable semiquinone of Complex III (Fig. 9D). Only the simulated rate of ROS generation by reduced $FMNH^-$ of Complex I is considerably increased at $v_{40} = 0$ in the presence of succinate (Fig. 9B). However, this increase does not compensate for the decrease in ROS production at the other two sites of $O_2^{\cdot-}$ formation. It should be noted that a decrease in the rate of ROS production by Complex III upon inhibition of cytochrome *c* oxidase by cyanide was observed in recent computational studies [23].

The strong decrease in the rate of ROS generation by the semiquinone of Complex I upon inhibition of cytochrome *c* oxidase during oxidation of succinate alone (Fig. 9C) deserves special attention. This additional site of ROS generation in Complex I is usually attributed to excessive ROS production during reverse electron transfer (RET). Therefore, at first glance, inhibition of cytochrome *c* oxidase should result in an increase in ROS generation at this site. However, this is not observed. The semiquinone concentration is held in equilibrium with both Q and QH_2. Upon inhibition of cytochrome *c* oxidase during oxidation of

succinate the concentration of oxidized Q approaches zero, because there is no respiration and no oxidation of QH_2 by Complex III. This results in a strong decrease in the concentration of the semiquinone in Complex I. In this case, almost all superoxide in Complex I is generated by reduced $FMNH^-$ (Fig. 9B). This result may account for recent experimental observations [79] that NADH and succinate, upon inhibition of cytochrome *c* oxidase by KCN, both induced ROS production by the same site, $FMNH^-$.

3.2.4. Depletion of cytochrome *c*

Experimental observations show that loss of cyt *c* from mitochondria results in a considerable increase in the ROS production rate with NADH-linked substrates [52, 80], whereas ROS decreases with succinate as electron donor [81]. We analyzed computationally the effects of cyt *c* depletion from the mitochondrial intermembrane space (IMS) on the ROS production rate by different sites of Complexes I and III during oxidation NADH alone and succinate alone. Fig. 10 presents the computer simulated ΔΨ dependency of the total ROS production rate (Fig. 10A) and ROS production at different sites of Complex I (Fig. 10B, C) and Complex III (Fig. 10D) with different cyt *c* concentrations, [Cyt c], in the IMS during the oxidation of NADH alone. The overall rate of ROS production (Fig. 10A) significantly increases upon extensive (more than 90%) depletion of cyt c at low membrane potential (ΔΨ < 120 mV), whereas practically no changes in ROS production occur at ΔΨ > 120 mV. It should be noted that the respiration rate becomes saturated at ΔΨ = 120 mV during oxidation of NADH alone (Fig. 3E). The considerable increase in the total ROS production rate upon complete cyt *c* depletion ([Cyt *c*]=0) results from a strong increase in $O_2^{\cdot-}$ formation by reduced $FMNH^-$ of Complex I (Fig. 10B). An increase in the ROS production rate at 0 < [Cyt *c*] < 70 μM and at ΔΨ < 120 mV occurs due to an increase in $O_2^{\cdot-}$ formation by the semiquinone of the Qo site (Fig.10D). Practically no changes in the ROS production rate occur at the semiquinone of Complex I (Fig. 10C) upon cyt *c* depletion.

By analogy, Fig. 11A–D presents the computer simulated rates of ROS production at different sites of the respiratory chain with different [Cyt *c]* during oxidation of succinate alone. In this case, the ROS production rate by the semiquinone of Complex I (Fig. 11C) decreases considerably with a decrease in [Cyt *c*], which results in a decrease in the total ROS production rate at ΔΨ > 140 mV (Fig. 11A). However, an increase in the total ROS production rate during oxidation of succinate alone occurs with cyt *c* depletion at ΔΨ < 140 mV due to an increase in $O_2^{\cdot-}$ formation by the unstable semiquinone of the Qo site of Complex III (Fig. 11D). It should be noted that the respiration rate becomes saturated at ΔΨ = 140 mV during oxidation of succinate alone (Fig. 3F). The rate of ROS generation by reduced $FMNH^-$ of Complex I increased with cyt *c* depletion (Fig. 11B).

Thus, the computer simulated responses to cyt *c* depletion are similar to those obtained upon inhibition of cytochrome c oxidase. This similarity is expected because inhibition of cytochrome *c* oxidase and cyt *c* depletion results in a similar reduction of electron carriers upstream of cyt *c*. The computational results presented are in agreement with experimental observations of the opposite effect of cyt *c* depletion on ROS production during NADH [52, 80] and succinate oxidation [81]. It is important to note that a decrease in ROS production with succinate alone probably occurs due to a decrease in ROS production by the

semiquinone of Complex I (Fig. 11C). An additional feature of cyt c depletion is the decrease in the rate of oxidation of superoxide anion to oxygen by cyt *c*, i.e. a decrease in scavenging of superoxide. However, an increase in the superoxide concentration that results from a scavenging decrease does not affect the rate of superoxide generation due to the low reversibility of this reaction.

3.2.5. The Q-dependence of $O_2^{\cdot-}$ production by antimycin-inhibited Complex III

Our previous analysis of computational models E and L was related mainly to steady state dependencies of the rates of respiration and $O_2^{\cdot-}$ production on membrane potential. However, recent experimental observations of unexpected non-monotonic dependencies of ROS production by Complex III in the presence of antimycin A (AA) on the activity of succinate dehydrogenase [17, 18] and the concentration of the oxidized ubiquinone Q [18] suggest it is important to pay more attention to the Q-dependence of $O_2^{\cdot-}$ production. Following Crofts and colleagues [12], we suggested in our current models that QH_2 and Q bind to the Qo site with oxidized cyt b_L only, i.e. we excluded the branch of QH_2 oxidation at the Qo site in which cyt b_L is reduced. This suggestion is supported in part by the work [17] published recently by Brand and coworkers. These authors showed that QH_2 oxidation by the branch in which QH_2 binds to the Qo site at reduced cyt b_L should occur with a very slow rate in order to account for their experimental data [17]. However, binding of Q to the Qo site at reduced cyt b_L has to be taken into consideration in order to account for some experimental data on ROS production by AA-inhibited Complex III, especially, the non-monotonic dependencies of ROS production on the concentration of respiratory substrates and oxidized Q. Previous experimental observations [17, 18, 82] showed that ROS production by AA-inhibited Complex III in the presence of a high concentration of succinate was enhanced by malonate, a competitive inhibitor of succinate dehydrogenase. Moreover, ROS production by AA-inhibited Complex III showed a non-monotonic dependence on the concentration of different respiratory substrates for Complexes I and III and the redox states of cyt b_L [17] and ubiquinone Q pool [18]. An initial increase in ROS production by antimycin-inhibited Complex III with increasing concentrations of different respiratory substrates and ubiquinol QH_2, respectively, can be understood intuitively because addition of respiratory substrates supplies electrons to the redox centers of Complex III, including the ROS producing unstable semiquinone. Therefore, the concentration of unstable semiquinone should increase with increasing concentrations of these substrates. However, a further unexpected decrease in ROS production at a high concentration of respiratory substrates, i.e. with a high QH_2/Q ratio, is harder to explain in the framework of the generally accepted concept that ubisemiquinone is formed during ubiquinol oxidation only. Therefore, in order to account for a decrease in ROS production by antimycin-inhibited Complex III with increasing QH_2/Q ratio (and an increase in ROS production with increasing oxidized ubiquinone Q) Drose and Brandt [18] proposed that oxidized ubiquinone supports ubisemiquinone formation and, respectively, superoxide production at the Qo site due to transfer of electrons from reduced cyt b_L onto Q in a reverse reaction of the Qo site. In models E and L, this is the reverse direction of reaction (24) presented in Fig. 1 and Fig. 2A. This implies that, in order to force this reverse reaction of electron transfer from reduced cyt b_L onto Q and increase superoxide production, free oxidized coenzyme Q has to support formation of the complex of Q with reduced cyt b_L, i.e. complexes b_L^-.Q and b_L^-.Q.ISPH in

Fig. 1 and Fig. 2A, respectively, as substrates of reaction (24) taken in the reverse direction. In models E and L, this is impossible for the following reason. Binding of free oxidized coenzyme Q to the Qo site in both E and L models occurs in the reverse direction of reaction (26) in Fig. 1 and 2A, which is downstream of reaction (25) of electron transfer from cyt b_L to cyt b_H, i.e. when cyt b_L is oxidized. This means that, in order to increase the concentration of free oxidized ubiquinone Q would result in increasing the concentration of complexes b_L^-.Q and b_L^-.Q.ISPH, respectively, in Fig. 1 and Fig. 2A, electron transfer from cyt b_H to cyt b_L in the reverse direction of reaction (25) should occur. However, we suggested earlier in Section 3.2.1 that reaction (25) is depressed in both forward and reverse directions in the presence of AA. This means that in models E and L, an increase in the free oxidized ubiquinone Q concentration cannot result in an increase in the ubisemiquinone formation and ROS production by AA-inhibited Complex III due to the reversal of reaction (24). Therefore, we extended model L and suggest that the free oxidized ubiquinone Q can bind to the Qo site when cyt b_L is reduced. In other words, we considered a new branched model in which coenzyme Q can bind/leave the Qo site before electron transfer from b_L to b_H occurs (the reversible reaction (41) presented in the modified kinetic scheme in Fig. 2B). The branched kinetic scheme of the Q-cycle presented in Fig. 2B takes into account the consecutive release of Q and ISPH from the Qo site and differs from the kinetic scheme presented in Fig. 2A by additional reactions (41), (42), (25a) and (34a). A mathematical model corresponding to this branched kinetic scheme (Fig. 2B) is presented in Supplementary data. Some of the steady state characteristics of this mathematical model based on the assumption that $v_{34}=v_{34a}=0$ in the presence of AA are presented in Fig. 12. Fig. 12A shows that the modified branched model describes qualitatively the experimentally observed non-monotonic dependence of ROS production on the activity of succinate dehydrogenase (Complex II) [17, 18] simulated in the model as changes in the maximal rate of Complex II, V_{max19} (see reaction (19) in Table 1). The mechanism responsible for the bell-shaped dependence of the rate of ROS production can be understood from the data shown in Fig. 12B, which presents the relationship between the maximal rate of Complex II, the fractions of oxidized ubiquinone Q and reduced cyt b_L, and the concentration of complex b_L^-.Q.ISPH, i.e., the substrate for the formation of semiquinone at the Qo site in the reverse direction of reaction (24). The ternary complex b_L^-.Q.ISPH is a product of three simultaneous events, namely, Rieske iron-sulfur protein ISP and cyt b_L have to be in the reduced form and ubiquinone Q in the oxidized state. Let us consider only changes in the steady state fractions of the reduced cyt b_L and oxidized ubiquinone Q, as the donor-acceptor pair in this complex, when the maximal rate of Complex II changes. Fig. 12B shows that the fraction of reduced cyt b_L and oxidized ubiquinone Q changes reciprocally with changes in the maximal rate of Complex II. This feature is the main reason for the non-monotonic dependence of ROS production on the maximal rate of Complex II shown in Fig. 12A. At a low rate of Complex II, when the Q pool and cyt b_L are mainly in the oxidized state, the concentration of the complex b_L^-.Q.ISPH is very low due to low levels of reduced cyt b_L (Fig. 12B). By analogy, complex b_L^-.Q.ISPH approaches zero at very high rates of Complex II due to the fraction of oxidized ubiquinone Q being negligible. Therefore, the steady state dependence of the concentration of the complex b_L^-.Q.ISPH on the maximal rate of Complex II is non-monotonic with a peak concentration of about 4 μM when the maximal rate of Complex II is around 60 μM/s, near the intersection point of the curves for

the reduced cyt b_L and oxidized ubiquinone Q fractions (Fig. 12B). For similar reasons, the steady state dependence of the concentration of complex b_L.QH2.ISPox on the maximal rate of Complex II is also non-monotonic, due to the reciprocal changes in oxidized cyt b_L and reduced ubiquinone QH_2 with changes in the maximal rate of Complex II. It should point out that complex b_L.QH2.ISPox is the substrate for semiquinone formation during ubiquinol oxidation in reaction (23) (Fig. 2B). Peak values of the complex b_L.QH2.ISPox concentration about 240 μM at the same values of the maximal rate of Complex II of 60 μM/s as for the complex b_L^-.Q.ISPH (data not shown). Since the semiquinone concentration at the Qo site, the $b_L.Q^{\cdot-}$.ISPH complex, is held in equilibrium with the both b_L.QH2.ISPox and b_L^-.Q.ISPH complexes, it is easy to understand that the concentration of the $b_L.Q^{\cdot-}$.ISPH complex and superoxide production by this complex follows the concentration of both the b_L.QH2.ISPox and b_L^-.Q.ISPH complexes and changes non-monotonically with changes in the maximal rate of Complex II as shown in Fig. 12A. This is true especially in the presence of AA when the respiration rate is very low and redox centers in Complex III are in the quasi-stationary state close to equilibrium. In addition, computer simulation also shows a bell-shaped dependence of superoxide production by the AA-inhibited Complex III on the relative fraction of the oxidized ubiquinone Q (Fig. 12C) and reduced cyt b_L (Fig. 12D), compatible with the experimentally observed nonmonotonic dependencies of ROS production on the redox states of ubiquinone Q pool [18] and cyt b_L [17]. However, further computer fitting procedure will be needed to account quantitatively for these experimentally observed dependencies. All computational results presented in Fig. 12 were obtained at $\Delta\Psi = 0$ and $v_{34} = v_{34a} = 0$ in order to simulate the effect of AA. It should be pointed out that changes in the oxidized ubiquinone Q and reduced cyt b_L fractions presented on the x-axis in Fig. 12C and 12D were obtained in the steady state of the branched model assuming changes in the maximal rate of Complex II. This means that changes in the steady state fraction of the oxidized ubiquinone Q (reduced cyt b_L) are accompanied by simultaneous reciprocal changes in reduced cyt b_L (oxidized Q), as shown in Fig. 12B, i.e. maximal steady state values of oxidized Q (reduced cyt b_L) correspond to minimal values of reduced cyt b_L (oxidized Q). This is the underlying reason for the non-monotonic dependence of ROS production in the branched model when it is plotted against the relative fraction of the oxidized ubiquinone Q (Fig. 12C) and reduced cyt b_L (Fig. 12D).

We evaluated how these additional steps in the modified branched model affect the results reported above with models E and L under uninhibited conditions and, especially, upon inhibition of reactions downstream of Complex III. A comparison of the computational results from model L and the modified branched model shows that they are quantitatively very close, both with and without inhibition of cytochrome *c* oxidase (Supplemental Fig. S5). However, the superoxide production rate in the branched model differs quantitatively from the rate in model L upon inhibition of Complex III by AA (Supplemental Fig. S6). The qualitative features of the curves of superoxide production in the both models are similar, however, i.e. the superoxide production rate increases with decreasing membrane potential, in agreement with experimental data [64]. The decrease in superoxide production by AA-inhibited Complex III in the branched model compared to the model L relates to a decrease in the concentration of the $O_2^{\cdot-}$ producing site complex $b_L.Q^{\cdot-}$.ISPH (Fig. 2B), reflecting the additional outflow of oxidized Q from the Qo site in the reaction (41). Thus, reaction (41)

plays an important role in the increase in $O_2^{\cdot-}$ production by Complex III at partial oxidation of the Q pool, due to reverse electron transfer from reduced cyt b_L to oxidized Q in reaction (24) in Fig. 2B, as was suggested earlier by different authors [18, 83].

In addition, we should point out that both the branched model and model L exclude a short circuit in the Q-cycle because these models are based on the experimentally supported hypothesis [11] that suggests that dissociation of ISPH from the Qo site occurs only after the second electron transfers from cyt b_L to b_H (reaction (26) in Figs 2A, B). In this case, the rate of respiration in the electron transport chain inhibited by AA closely matches the rate of $O_2^{\cdot-}$ production by complex $b_L.Q^{\cdot-}$.ISPH. This results from the suggestion that $v_{34}=0$ and $v_{34}=v_{34a}=0$ in model L and the branched model, respectively, simulating inhibition of the Qi site by AA. (For further detail, see the mathematical models corresponding to different kinetic schemes in Supplementary data). However, some authors [83] experimentally observed a reduction of cyt *c* by the AA-inhibited cytochrome bc_1 complex with a rate that did not depend on the rate of $O_2^{\cdot-}$ production, which implies a short circuit in the Q-cycle. Therefore, we cannot exclude the possibility that the kinetic scheme of the favorable branched model presented in Fig. 2B can be extended due to additional reactions involving, in particular, a slow dissociation of ISPH from the Qo site before the second electron transfers from cyt b_L to b_H, i.e. slow ISPH dissociation from complexes b_L^{-}.ISPH and $b_L.Q^{\cdot-}$.ISPH. This additional slow dissociation of reduced ISPH would be followed by its oxidation by cyt c_1 and a return of oxidized ISPox to the Qo site, where it would accept the second electron from the $O_2^{\cdot-}$ forming unstable semiquinone to produce the second molecule of reduced ISPH. This mechanism can, first, explain a possible slow short-circuit when both electrons transfer from QH_2 into the high potential *c*-chain [13] and, second, develop an additional mechanism to control $O_2^{\cdot-}$ production by Complex III.

4. Conclusions

In this paper, we have developed a computational model of superoxide formation in the mitochondrial electron transport chain based on a detailed kinetic scheme of the electron transfer reactions in Complex I and III. The model has the flexibility to account for multiple, often seemingly contradictory observations on the effects of ΔΨ and ΔpH, as well as for the effects of multiple substrate and inhibitor conditions reported on the literature. Table 3 summarizes the ROS production rates under different substrate and inhibitor conditions and the contribution of the different ETC sites considered. The major important findings highlighted in our analyses can be summarized as follows:

The computational model accounts for experimentally observed ΔΨ dependency of the ROS production rate with different respiratory substrates and supports a hypothesis about the semiquinone of Complex I as an additional $O_2^{\cdot-}$ generating site

Our computational modeling results confirm the very high ΔΨ sensitivity of the ROS production rate observed experimentally [57] and theoretically [23] in mitochondria using succinate or NADH-linked respiratory substrates [7, 55, 56] and predict also the strong ΔΨ-dependency of ROS production for NADH + succinate oxidation (Fig. 3). Moreover, the computer simulation (Fig. 3A, D) shows that the ROS production rate by Complex I for

NADH oxidation becomes independent of ΔΨ upon rotenone application, which is compatible with experimental observations [40, 41] showing that uncouplers don't affect ROS generation upon oxidation of NADH-linked respiratory substrates in the presence of rotenone. A strong increase in ROS production supported by different respiratory substrates at high ΔΨ is accounted for essentially by an increase in the concentration of the ubisemiquinone radical of Complex I (Fig. 3B), which has a very high $\Delta\mu_H$ sensitivity, as observed experimentally [37, 38]. Consideration of the ubisemiquinone radical (complex CI.$Q^{\cdot-}$ in Fig. 1) as an additional $O_2^{\cdot-}$ generating site in Complex I is not supported by direct experimental observations although our computer simulation results and numerous experimental data [7, 9, 10] indirectly support this hypothesis. Elimination of this site in our computer simulation would disregard the ROS generation rate in the presence of succinate alone, i.e. during reversible electron transfer (RET), which would contradict experimental observations [6]. However, under certain special conditions of RET, e.g. upon inhibition of Complex III (Fig. 7C) or cytochrome *c* oxidase (Fig. 9C), oxidation of succinate alone results in inhibition of ROS production by the semiquinone of Complex I. Therefore, almost all superoxide in Complex I is generated by reduced $FMNH^-$ upon inhibition of Complex III (Fig. 7B) or cytochrom *c* oxidase (Fig. 9B). This results matches the properties of $NADH^-$ and RET-induced ROS production that were observed experimentally [79]. In this context, it should be also pointed out that ROS production is strongly inhibited by free fatty acids (FFA) in the presence of succinate alone [84]. These authors [84] noted that FFA have a dual effect, first, depolarization of the inner membrane due to their uncoupling effect and, second, partly blocking the respiratory chain, likely at the level of Complex III, and suggested that FFA decrease ROS generation during RET due to their uncoupling action. This is compatible with our modeling results presented in Fig. 3B that superoxide formation by the ubisemiquinone radical of Complex I, as the main ROS-producing site during RET, is strongly depressed upon depolarization of the inner membrane. In addition, we should point out that blocking Complexes III and IV also strongly depresses ROS production by the ubisemiquinone radical of Complex I (Fig. 7C and 9C) during RET. This suggests that the experimentally observed FFA inhibition of ROS production during RET could be accounted for both by depolarization of the inner membrane and by partly inhibition of the respiratory chain.

The sequential mechanism of QH_2 oxidation with late dissociation of ISPH is more likely

Computer simulation of inhibition of Complex III by AA and myxothiazol in models with early [12] (model E) and late [11] (model L) dissociation of ISPH from cyt b_L shows that model L is preferred for the following reasons. First, it is well known that AA induces an increase in the ROS production rate. Moreover, experimental observations [85] show that the uncoupler FCCP increases the AA induced ROS generation at the Qo site of complex III. This is not compatible with model E, in which AA induced ROS production drops to 0 at a low membrane potential. Besides, the computer simulated effect of inhibition of the second electron transfer in the Qo site (v_{24}=0) on the ROS production rate fits the experimentally observed effect of myxothiazol and not that of stigmatellin. This conclusion is very important because model L has a FeS-lock mechanism to protect Complex III from short-circuiting when both electrons transfer from QH_2 into the high potential *c*-chain [13].

Myxothiazol inhibits the second electron transfer in the Qo site

Computer simulated results presented in Fig. 7A,C support the hypothesis suggested by Yu and others [11] that myxothiazol inhibits transfer of the second electron from the ubisemiquinone radical to cyt b_L. Inhibition of this step by myxothiazol has an effect on the ROS production rate that is identical to the effect of AA in model L (Fig. 5B,D) which is compatible with experimental observations of the myxothiazol effect on ROS production in liver mitochondria [71]. However, there are experimental observations in rat heart and brain [70] and insect muscle [86] mitochondria which showed a smaller increase in ROS production induced by myxothiazol alone than AA alone. Moreover, these observations show inhibition of the ROS production rate by myxothiazol in the presence of AA. One of the reasons for this may be inhibition of Complex I by myxothiazol [87]. Another reason may be competitive inhibition by myxothiazol of binding of quinol QH_{2p} to the Qo site (reaction (22)) (see Supplementary Fig. S3).

ROS production by the ETC has a complex dependency on ΔΨ that varies with the concentration and nature of respiratory substrates and the presence of inhibitors

The generally accepted explanation that ΔΨ-dependencies of the rates of respiration and ROS production are reciprocal, i.e. that ROS production rates decrease upon depolarization of the inner membrane, does not give an accurate description of the complexity of the control of these processes. Under some conditions, e.g. for the $FMNH^-$ site with NADH as a substrate in the absence of rotenone, a high ROS production rate at a high ΔΨ can result from a more reduced carriers of ETC at the low respiration rate observed in state 4 respiration. However, in general the situation will be more complex and an analysis of ΔΨ-dependency of ROS production by different sites of ETC should be done separately for each site.

IMM depolarization of the inner mitochondrial membrane inhibits ROS production by both Complex I sites, $FMNH^-$ and $CI.Q^{\cdot-}$ during oxidation of any substrates in the absence of inhibitors of the ETC (Fig. 3A, B). This is easy to understand because both these sites, $FMNH^-$ and $CI.Q^{\cdot-}$, are upstream of the potential-dependent transfer of four protons into the IMS in reaction (13). A high ΔΨ promotes an increase in their concentration at these sites, especially for the $CI.Q^{\cdot-}$ site [37, 38]. Therefore, the concentration of these sites should decrease with decreasing membrane potential. However, during oxidation of Succ alone the steady state electron transfer in Complex I is close to equilibrium (apart from a minor deviation from equilibrium due to bypass reactions (16) and (17) of superoxide formation (Fig. 1, 2)). In this case, ROS production is maximal at high values of membrane potential. Addition of NADH stimulates forward electron transfer in Complex I with a transition from the near-equilibrium to the stationary state, resulting in a strong depression of ROS production at the $CI.Q^{\cdot-}$site(Fig. 3B, NADH+Succ).

The ΔΨ-dependency of ROS production by the unstable semiquinone of Complex III, the complex $b_L.Q^{\cdot-}$.ISPH, is more complex and depends non-monotonically on the rate of oxidation of any substrates in the absence of inhibitors of the ETC (Fig. 3C). This is due to the following: In the absence of inhibitors of the ETC, the steady state rate of transfer of electrons through complex $b_L.Q^{\cdot-}$.ISPH during oxidation of NADH, Succ or NADH+Succ

occurs mainly in the forward direction of reaction (24) with rate v_{24}. This rate is approximately equal to the respiration rate (v_{resp}), suggesting that the bypass reactions in Complex III are slow compared to the respiratory rate. Therefore, the concentration of complex $b_L.Q^{\cdot-}$.ISPH is proportional to the respiration rate (since $v_{resp} \sim v_{24} \sim k_{24} \cdot [b_L.Q^{\cdot-}.ISPH]$ in the steady state). This implies that the steady state concentration $[b_L.Q^{\cdot-}.ISPH]$ adapts to the steady state respiratory rate, which strongly increases upon depolarization of the inner membrane (or is depressesed at high values of $\Delta\Psi$). For instance, compare simulated ROS formation at $100 \leq \Delta\Psi \leq 180$ mV during oxidation of NADH+Succ in Fig. 3E. This is the main reason of the initial increase in computer simulated ROS production by Complex III upon depolarization of the inner membrane at $100 \leq \Delta\Psi \leq 180$ mV during oxidation of NADH+Succ in Fig. 3C. Further depolarization of the membrane below approximately 100 mV results in saturation of the respiratory rate (Fig. 3E, NADH +Succ) and a decrease in ROS production by Complex III (Fig. 3C, NADH+Succ), which is due to a strong oxidation of the Q pool and a decrease in the concentration of complex $b_L.Q^{\cdot-}$.ISPH. It should be noted that the $\Delta\Psi$-dependency of ROS production by the unstable semiquinone of Complex III, i.e., complex $b_L.Q^{\cdot-}$.ISPH, during oxidation of Succ alone is almost monotonic and decreases upon depolarization. This is compatible with both experimentally observed [56] and computer simulated [23] results.

A comment on changes in the mitochondrial membrane potential

We analyzed steady state characteristics of ROS production in the electron transport chain under uninhibited conditions and upon inhibition of different segments of the respiratory chain at fixed values of the membrane potential. We did not consider explicitly alterations in membrane potential during inhibition of the respiratory chain. Alterations in the mitochondrial membrane potential *in vivo* depend on the activity of numerous electrogenic transport systems in the inner mitochondrial membrane such as Ca^{2+}- and K^+-channels, adenine nucleotide translocase, electrogenic H^+ transport systems including H^+ leak and H^+ pumps of F_0F_1-ATPase and Complexes I, III and IV of the respiratory chain. Therefore, it would be expected that a decrease in the membrane potential occurs after inhibition of the respiratory chain and its H^+ pumps unless $\Delta\Psi$ is maintained by other reactions. However, real alterations in membrane potential are hard to assess because they depend on the activity of mitochondrial electrogenic transport systems apart from the electron transport chain. Therefore, we analyzed steady state ROS production over a wide range of $\Delta\Psi$ in order to take into account any possible alterations in $\Delta\Psi$ upon inhibition of the respiratory chain and extrapolated the rates of ROS production under different condition to any values of $\Delta\Psi$.

Testable predictions

In summary, the computational model developed here can be used to make experimentally verifiable and mechanistically sound predictions on the rates of ROS production at different sites of the electron transport chain. Our computational results predict that superoxide formation in Complex I during oxidation of succinate (RET) occurs predominantly at the semiquinone of Complex I, if no inhibitors of the respiratory chain are present (Fig. 3A–D). Therefore, inhibition of the flavin site of Complex I generally should not affect ROS production during succinate oxidation, i.e. during RET in the absence of any inhibitors of Complexes III and IV. By contrast, inhibitors of the flavin site should largely abolish ROS

production during RET in the presence of inhibitors of cytochrome *c* oxidase. The rate of ROS generation by the semiquinone of Complex I during RET can be quantified using inhibitors of both flavin and Q-binding sites of Complex I. In accord with our model, superoxide formation occurs only at the semiquinones of Complexes I and III in the presence of flavin site inhibitors (e.g., NADH-OH, ADP-ribose, DPI). The rate of ROS generation by Complex III during RET can be found in the presence of rotenone, the inhibitor of Complex I. Therefore, in order to find the ROS production rate generated by the semiquinone of Complex I during RET, the rate of ROS production in the presence of rotenone should be subtracted from the rate of ROS production in the presence of an inhibitor of flavin site. The model can similarly be used to predict the consequences for mitochondrial ROS production of changes in the expression level or activity of specific components of the electron transport chain e.g., as a consequence of signaling processes impacting respiratory complexes, or associated with specific disease conditions. Importantly, in our studies we focused on the ETC-dependent processes that generate superoxide. It should be emphasized that the net rate of ROS production in intact cells and tissues is strongly dependent on the activity of multiple oxidative stress defense mechanisms available both in the mitochondrial matrix and in other compartments in all cells. A detailed understanding of the balance of mitochondrial ROS production and its biological effects needs to take account of these and related antioxidant contributions to net ROS production (e.g., see [23]).

Supplementary Material

Refer to Web version on PubMed Central for supplementary material.

Acknowledgements

This work was supported by NIH grants K25 AA016604 (NIM) and R01 AA015311 (JBH). and Grant of government of Russian Federation № 14.Z50.31.0028.

References

1. Dröge W. Free radicals in the physiological control of cell function. Physiol. Rev. 2002; 82:47–95. [PubMed: 11773609]
2. Schieber M, Chandel NS. ROS function in redox signaling and oxidative stress. Curr Biol. 2014; 24:R453–R462. [PubMed: 24845678]
3. Ye ZW, Zhang J, Townsend DM, Tew KD. Oxidative stress, redox regulation, and diseases of cellular differentiation. Biochim. Biohys. Acta. Nov 15.2014 S0304-4165(14) 00387-0. doi: 10.1016. [Epub ahead of print].
4. Boveris A, Chance B. The mitochondrial generation of hydrogen peroxide. General properties and effect of hyperbaric oxygen. Biochem. J. 1973; 134:707–716. [PubMed: 4749271]
5. Hirst J. Mitochondrial complex I. Annu. Rev. Biochem. 2013; 82:551–575. [PubMed: 23527692]
6. Hirst J, King MS, Pryde KR. The production of reactive oxygen species by complex I. Biochem. Soc. Trans. 2008; 36:976–980. [PubMed: 18793173]
7. Lambert AJ, Brand MD. Inhibitors of the quinone-binding site allow rapid superoxide production from mitochondrial NADH:ubiquinone oxidoreductase (complex I). J. Biol. Chem. 2004; 279:39414–39420. [PubMed: 15262965]
8. Crofts AR, Lhee S, Crofts SB, Cheng J, Rose S. Proton pumping in the bc1 complex: a new gating mechanism that prevents short circuits. Biochim. Biophys. Acta. 2006; 1757:1019–1034. [PubMed: 16600173]

9. Ohnishi ST, Shinzawa-Itoh K, Ohta K, Yoshikawa S, Ohnishi T. New insights into the superoxide generation sites in bovine heart NADH-ubiquinone oxidoreductase (Complex I): the significance of protein-associated ubiquinone and the dynamic shifting of generation sites between semiflavin and semiquinone radicals. Biochim. Biophys. Acta. 2010; 1797:1901–1909. [PubMed: 20513438]
10. Treberg JR, Quinlan CL, Brand MD. Evidence for two sites of superoxide production by mitochondrial NADH-ubiquinone oxidoreductase (complex I). J. Biol. Chem. 2011; 286:27103–27110. [PubMed: 21659507]
11. Yu CA, Cen X, Ma HW, Yin Y, Yu L, Esser L, Xia D. Domain conformational switch of the iron-sulfur protein in cytochrome bc1 complex is induced by the electron transfer from cytochrome bL to bH. Biochim. Biophys. Acta. 2008; 1777:1038–1043. [PubMed: 18452702]
12. Crofts AR, Hong S, Wilson C, Burton R, Victoria D, Harrison C, Schulten K. The mechanism of ubihydroquinone oxidation at the Qo-site of the cytochrome bc1 complex. Biochim. Biophys. Acta. 2013; 1827:1362–1377. [PubMed: 23396004]
13. Mulkidjanian AY. Ubiquinol oxidation in the cytochrome bc1 complex: reaction mechanism and prevention of short-circuiting. Biochim. Biophys. Acta. 2005; 1709:5–34. [PubMed: 16005845]
14. Link TA. The role of the 'Rieske' iron sulfur protein in the hydroquinone oxidation (Q(P)) site of the cytochrome bc1 complex. The 'proton-gated affinity change' mechanism. FEBS Lett. 1997; 412:257–264. [PubMed: 9256231]
15. Zhu J, Egawa T, Yeh SR, Yu L, Yu CA. Simultaneous reduction of iron-sulfur protein and cytochrome b(L) during ubiquinol oxidation in cytochrome bc(1) complex. Proc. Natl. Acad. Sci. U S A. 2007; 104:4864–4869. [PubMed: 17360398]
16. Xia D, Esser L, Yu L, Yu CA. Structural basis for the mechanism of electron bifurcation at the quinol oxidation site of the cytochrome bc1 complex. Photosynth. Res. 2007; 92:17–34. [PubMed: 17457691]
17. Quinlan CL, Gerencser AA, Treberg JR, Brand MD. The mechanism of superoxide production by the antimycin-inhibited mitochondrial Q-cycle. J. Biol. Chem. 2011; 286:31361–31372. [PubMed: 21708945]
18. Drose S, Brandt U. The mechanism of mitochondrial superoxide production by the cytochrome bc1 complex. J. Biol. Chem. 2008; 283:21649–21654. [PubMed: 18522938]
19. Selivanov VA, Votyakova TV, Zeak JA, Trucco M, Roca J, Cascante M. Bistability of mitochondrial respiration underlies paradoxical reactive oxygen species generation induced by anoxia. PLoS Comput. Biol. 2009; 5:e1000619. [PubMed: 20041200]
20. Selivanov VA, Votyakova TV, Pivtoraiko VN, Zeak J, Sukhomlin T, Trucco M, Roca J, Cascante M. Reactive oxygen species production by forward and reverse electron fluxes in the mitochondrial respiratory chain. PLoS Comput. Biol. 2011; 7:e1001115. [PubMed: 21483483]
21. Demin OV, Kholodenko BN, Skulachev VP. A model of O2.-generation in the complex III of the electron transport chain. Mol. Cell. Biochem. 1998; 184:21–33. [PubMed: 9746310]
22. Orii Y, Miki T. Oxidation process of bovine heart ubiquinol-cytochrome c reductase as studied by stopped-flow rapid-scan spectrophotometry and simulations based on the mechanistic Q cycle model. J. Biol. Chem. 1997; 272:17594–17604. [PubMed: 9211907]
23. Gauthier LD, Greenstein JL, Cortassa S, O'Rourke B, Winslow RL. A computational model of reactive oxygen species and redox balance in cardiac mitochondria. Biophys. J. 2013; 105:1045–1056. [PubMed: 23972856]
24. Bazil JN, Vinnakota KC, Wu F, Beard DA. Analysis of the kinetics and bistability of ubiquinolxytochrome c oxidoreductase. Biophys. J. 2013; 105:343–355. [PubMed: 23870256]
25. Zoladz B, Korzeniewski JA. A model of oxidative phosphorylation in mammalian skeletal muscle. Biophys. Chem. 2001; 92:17–34. [PubMed: 11527576]
26. Beard DA. A biophysical model of the mitochondrial respiratory system and oxidative phosphorylation. PLoS Comput. Biol. 2005; 1:e36. [PubMed: 16163394]
27. Markevich NI, Hoek JB. Computational analysis of hysteresis and bistability in the mitochondrial respiratory chain. Math. Biol. Bioinformatics. 2014; 9:89–111.
28. Kussmaul L, Hirst J. The mechanism of superoxide production by NADH:ubiquinone oxidoreductase (complex I) from bovine heart mitochondria. Proc. Natl. Acad. Sci U S A. 2006; 103:7607–7612. [PubMed: 16682634]

29. Vinogradov AD. NADH/NAD+ interaction with NADH: ubiquinone oxidoreductase (complex I). Biochim Biophys Acta. 2008; 1777:729–734. [PubMed: 18471432]
30. Birrell JA, Yakovlev G, Hirst J. Reactions of the flavin mononucleotide in complex I: combined mechanism describes NADH oxidation coupled to the reduction of APAD+, ferricyanide, or molecular oxygen. Biochemistry. 2009; 48:12005–12013. [PubMed: 19899808]
31. Ransac S, Heiske M, Mazat JP. From in silico to in spectro kinetics of respiratory complex I. Biochim. Biophys. Acta. 2012; 1817:1958–1969. [PubMed: 22510388]
32. Brandt U. Energy converting NADH:quinone oxidoreductase (complex I). Annu. Rev. Biochem. 2006; 75:69–92. [PubMed: 16756485]
33. Moser CC, Farid TA, Chobot SE, Dutton PL. Electron tunneling chains of mitochondria. Biochim. Biophys. Acta. 2006; 1757:1096–1109. [PubMed: 16780790]
34. Verkhovskaya ML, Belevich N, Euro L, Wikstrom M, Verkhovsky MI. Real-time electron transfer in respiratory complex I. Proc. Natl. Acad. Sci U S A. 2008; 105:3763–3767. [PubMed: 18316732]
35. Ransac S, Arnarez C, Mazat JP. The flitting of electrons in complex I: a stochastic approach. Biochim. Biophys. Acta. 2010; 1797:641–648. [PubMed: 20230777]
36. Efremov RG, Baradaran R, Sazanov LA. The architecture of respiratory complex I. Nature. 2010; 465:441–445. [PubMed: 20505720]
37. Vinogradov AD, Sled VD, Burbaev DS, Grivennikova VG, Moroz IA, Ohnishi T. Energy-dependent Complex I-associated ubisemiquinones in submitochondrial particles. FEBS Lett. 1995; 370:83–87. [PubMed: 7649309]
38. Magnitsky S, Toulokhonova L, Yano T, Sled VD, Hagerhall C, Grivennikova VG, Burbaev DS, Vinogradov AD, Ohnishi T. EPR characterization of ubisemiquinones and iron-sulfur cluster N2 central components of the energy coupling in the NADH-ubiquinone oxidoreductase (complex I) in situ. J. Bioenerg. Biomembr. 2002; 34:193–208. [PubMed: 12171069]
39. Kao MC, Nakamaru-Ogiso E, Matsuno-Yagi A, Yagi T. Characterization of the membrane domain subunit NuoK (ND4L) of the NADH-quinone oxidoreductase from Escherichia coli. Biochemistry. 2005; 44:9545–9554. [PubMed: 15996109]
40. Votyakova TV, Reynolds IJ. DeltaPsi(m)-Dependent and -independent production of reactive oxygen species by rat brain mitochondria. J. Neurochem. 2001; 79:266–277. [PubMed: 11677254]
41. Vinogradov AD, Grivennikova VG. Generation of superoxide-radical by the NADH:ubiquinone oxidoreductase of heart mitochondria. Biochemistry (Mosc.). 2005; 70:120–127. [PubMed: 15807648]
42. Raha S, Robinson BH. Mitochondria, oxygen free radicals, disease and ageing. Trends Biochem. Sci. 2000; 25:502–528. [PubMed: 11050436]
43. Mitchell P. Protonmotive redox mechanism of the cytochrome b-c1 complex in the respiratory chain: protonmotive ubiquinone cycle. FEBS Lett. 1975; 56:1–6. [PubMed: 239860]
44. Zhang Z, Huang L, Shulmeister VM, Chi YI, Kim KK, Hung LW, Crofts AR, Berry EA, Kim SH. Electron transfer by domain movement in cytochrome bc1. Nature. 1998; 392:677–684. [PubMed: 9565029]
45. Cape JL, Bowman MK, Kramer DM. A semiquinone intermediate generated at the Qo site of the cytochrome bc1 complex: importance for the Q-cycle and superoxide production. Proc. Natl. Acad. Sci. U S A. 2007; 104:7887–7892. [PubMed: 17470780]
46. Muller FL, Liu Y, Van Remmen H. Complex III releases superoxide to both sides of the inner mitochondrial membrane. J. Biol. Chem. 2004; 279:49064–49073. [PubMed: 15317809]
47. Deichmann U, Schuster S, Mazat JP, Cornish-Bowden A. Commemorating the 1913 Michaelis-Menten paper Die Kinetik der Invertinwirkung: three perspectives. FEBS J. 2014; 281:435–463. [PubMed: 24180270]
48. Vinnakota KC, Bassingthwaighte JB. Myocardial density and composition: a basis for calculating intracellular metabolite concentrations. Am. J. Physiol. Heart Circ. Physiol. 2004; 286:H1742–H1749. [PubMed: 14693681]
49. Hackenbrock CR, Chazotte B, Gupte SS. The random collision model and a critical assessment of diffusion and collision in mitochondrial electron transport. J. Bioenerg. Biomembr. 1986; 18:331–368. [PubMed: 3021714]

50. Wu F, Yang F, Vinnakota KC, Beard DA. Computer modeling of mitochondrial tricarboxylic acid cycle, oxidative phosphorylation, metabolite transport, and electrophysiology. J. Biol. Chem. 2007; 282:24525–24537. [PubMed: 17591785]
51. Schwerzmann K, Cruz-Orive LM, Eggman R, Sanger A, Weibel ER. Molecular architecture of the inner membrane of mitochondria from rat liver: a combined biochemical and stereological study. J. Cell. Biol. 1986; 102:97–103. [PubMed: 2867101]
52. Kushnareva Y, Murphy AN, Andreyev A. Complex I-mediated reactive oxygen species generation: modulation by cytochrome c and NAD(P)+ oxidation-reduction state. Biochem. J. 2002; 368:545–553. [PubMed: 12180906]
53. Kudin AP, Bimpong-Buta NY, Vielhaber S, Elger CE, Kunz WS. Characterization of superoxide-producing sites in isolated brain mitochondria. J. Biol. Chem. 2004; 279:4127–4135. [PubMed: 14625276]
54. Grivennikova VG, Vinogradov AD. Generation of superoxide by the mitochondrial Complex I. Biochim. Biophys. Acta. 2006; 1757:553–561. [PubMed: 16678117]
55. Starkov AA, Fiskum G. Regulation of brain mitochondrial H2O2 production by membrane potential and NAD(P)H redox state. J. Neurochem. 2003; 86:1101–1107. [PubMed: 12911618]
56. Rottenberg H, Covian R, Trumpower BL. Membrane potential greatly enhances superoxide generation by the cytochrome bc1 complex reconstituted into phospholipid vesicles. J. Biol. Chem. 2009; 284:19203–19210. [PubMed: 19478336]
57. Lambert AJ, Brand MD. Superoxide production by NADH:ubiquinone oxidoreductase (complex I) depends on the pH gradient across the mitochondrial inner membrane. Biochem. J. 2004; 382:511–517. [PubMed: 15175007]
58. Batandier C, Guigas B, Detaille D, El-Mir MY, Fontaine E, Rigoulet M, Leverve XM. The ROS production induced by a reverse-electron flux at respiratory-chain complex 1 is hampered by metformin. J. Bioenerg. Biomembr. 2006; 38:33–42. [PubMed: 16732470]
59. Hoffman DL, Brookes PS. Oxygen sensitivity of mitochondrial reactive oxygen species generation depends on metabolic conditions. J. Biol. Chem. 2009; 284:16236–16245. [PubMed: 19366681]
60. Chance B, Sies H, Boveris A. Hydroperoxide metabolism in mammalian organs. Physiol. Rev. 1979; 59:527–605. [PubMed: 37532]
61. Andreyev AY, Kushnareva YE, Starkov AA. Mitochondrial metabolism of reactive oxygen species. Biochemistry (Mosc.). 2005; 70:200–214. [PubMed: 15807660]
62. Murphy MP. How mitochondria produce reactive oxygen species. Biochem. J. 2009; 417:1–13. [PubMed: 19061483]
63. Aon MA, Stanley BA, Sivakumaran V, Kembro JM, O'Rourke B, Paolocci N, Cortassa S. Glutathione/thioredoxin systems modulate mitochondrial H2O2 emission: an experimental-computational study. J. Gen. Physiol. 2012; 139:479–491. [PubMed: 22585969]
64. Cadenas E, Boveris A. Enhancement of hydrogen peroxide formation by protophores and ionophores in antimycin-supplemented mitochondria. Biochem. J. 1980; 188:31–37. [PubMed: 7406888]
65. Tsai AL, Palmer G. The role of phospholipids in the binding of antimycin to yeast Complex III. Biochim. Biophys. Acta. 1986; 852:100–105. [PubMed: 3021213]
66. Kroger AA, Klingenberg M. Further evidence for the pool function of ubiquinone as derived from the inhibition of the electron transport by antimycin. Eur. J. Biochem. 1973; 39:313–323. [PubMed: 4359626]
67. Bechmann G, Weiss H, Rich PR. Non-linear inhibition curves for tight-binding inhibitors of dimeric ubiquinol-cytochrome c oxidoreductases. Evidence for rapid inhibitor mobility. Eur. J. Biochem. 1992; 208:315–325. [PubMed: 1325904]
68. Castellani M, Covian R, Kleinschroth T, Anderka O, Ludwig B, Trumpower BL. Direct demonstration of half-of-the-sites reactivity in the dimeric cytochrome bc1 complex: enzyme with one inactive monomer is fully active but unable to activate the second ubiquinol oxidation site in response to ligand binding at the ubiquinone reduction site. J. Biol. Chem. 2010; 285:502–510. [PubMed: 19892700]
69. Ransac S, Mazat JP. How does antimycin inhibit the bcl complex? A part-time twin. Biochim. Biophys. Acta. 2010; 1797:1849–1857. [PubMed: 20529661]

70. Starkov AA, Fiskum G. Myxothiazol induces H(2)O(2) production from mitochondrial respiratory chain. Biochem. Biophys. Res. Commun. 2001; 281:645–650. [PubMed: 11237706]
71. Young TA, Cunningham CC, Bailey SM. Reactive oxygen species production by the mitochondrial respiratory chain in isolated rat hepatocytes and liver mitochondria: studies using myxothiazol. Arch. Biochem. Biophys. 2002; 405:65–72. [PubMed: 12176058]
72. Sun J, Trumpower BL. Superoxide anion generation by the cytochrome bc1 complex. Arch. Biochem. Biophys. 2003; 419:198–206. [PubMed: 14592463]
73. Xia D, Yu CA, Kim H, Xia JZ, Kachurin AM, Zhang L, Yu L, Deisenhofer J. Crystal structure of the cytochrome bc1 complex from bovine heart mitochondria. Science. 1997; 277:60–66. [PubMed: 9204897]
74. Link TA, Haase U, Brandt U, von Jagow G. What information do inhibitors provide about the structure of the hydroquinone oxidation site of ubihydroquinone: cytochrome c oxidoreductase? J. Bioenerg. Biomembr. 1993; 25:221–232. [PubMed: 8394318]
75. Kim H, Xia D, Yu CA, Xia JZ, Kachurin AM, Zhang L, Yu L, Deisenhofer J. What information do inhibitors provide about the structure of the hydroquinone oxidation site of ubihydroquinone: cytochrome c oxidoreductase? Proc. Natl. Acad. Sci. U S A. 1998; 95:8026–8033. [PubMed: 9653134]
76. Dawson TL, Gores GJ, Nieminen AL, Herman B, Lemasters JJ. Mitochondria as a source of reactive oxygen species during reductive stress in rat hepatocytes. Am. J. Physiol. 1993; 264:C961–C967. [PubMed: 8386454]
77. Chen Q, Vazquez EJ, Moghaddas S, Hoppel CL, Lesnefsky EJ. Production of reactive oxygen species by mitochondria: central role of complex III. J. Biol. Chem. 2003; 278:36027–36031. [PubMed: 12840017]
78. Ambrosio G, Zweier JL, Duilio C, Kuppusamy P, Santoro G, Elia PP, Tritto I, Cirillo P, Condorelli M, Chiariello M, et al. Evidence that mitochondrial respiration is a source of potentially toxic oxygen free radicals in intact rabbit hearts subjected to ischemia and reflow. J. Biol. Chem. 1993; 268:18532–18541. [PubMed: 8395507]
79. Pryde KR, Hirst J. Superoxide is produced by the reduced flavin in mitochondrial complex I: a single, unified mechanism that applies during both forward and reverse electron transfer. J. Biol. Chem. 2011; 286:18056–18065. [PubMed: 21393237]
80. Pasdois P, Parker JE, Griffiths EJ, Halestrap AP. The role of oxidized cytochrome c in regulating mitochondrial reactive oxygen species production and its perturbation in ischaemia. Biochem. J. 2011; 436:493–505. [PubMed: 21410437]
81. Turrens JF, Alexandre A, Lehninger AL. Ubisemiquinone is the electron donor for superoxide formation by complex III of heart mitochondria. Arch. Biochem. Biophys. 1985; 237:408–414. [PubMed: 2983613]
82. Erecinska M, Wilson DF. The effect of antimycin A on cytochromes b561, b566, and their relationship to ubiquinone and the iron-sulfer centers S-1 (+N-2) and S-3. Arch. Biochem. Biophys. 1976; 174:143–157. [PubMed: 180891]
83. Sarewicz M, Borek A, Cieluch E, Swierczek M, Osyczka A. Discrimination between two possible reaction sequences that create potential risk of generation of deleterious radicals by cytochrome bc_1. Implications for the mechanism of superoxide production. Biochim. Biophys. Acta. 2010; 1797:1820–1827. [PubMed: 20637719]
84. Schonfeld P, Wojtczak L. Fatty acids decrease mitochondrial generation of reactive oxygen species at the reverse electron transport but increase it at the forward transport. Biochim. Biophys. Acta. 2007; 1767:1032–1040. [PubMed: 17588527]
85. Drose S, Hanley PJ, Brandt U. Ambivalent effects of diazoxide on mitochondrial ROS production at respiratory chain complexes I and III. Biochim. Biophys. Acta. 2009; 1790:558–565. [PubMed: 19364480]
86. Sohal RS. Aging, cytochrome oxidase activity, and hydrogen peroxide release by mitochondria. Free Radic. Biol. Med. 1993; 14:583–588. [PubMed: 8392019]
87. Degli Esposti M, Ghelli A, Crimi M, Estornell E, Fato R, Lenaz G. Complex I and complex III of mitochondria have common inhibitors acting as ubiquinone antagonists. Biochem. Biophys. Res. Commun. 1993; 190:1090–1096. [PubMed: 8439309]

88. Grivennikova VG, Vinogradov AD. Kinetics of ubiquinone reduction by the resolved succinate: ubiquinone reductase. Biochim. Biophys. Acta. 1982; 682:491–495. [PubMed: 7150582]

89. Sled VD, Rudnitzky NI, Hatefi Y, Ohnishi T. Thermodynamic analysis of flavin in mitochondrial NADH:ubiquinone oxidoreductase (complex I). Biochemistry. 1994; 33:10069–10075. [PubMed: 8060976]

90. Ohnishi T. Iron-sulfur clusters/semiquinones in complex I. Biochim. Biophys. Acta. 1998; 1364:186–206. [PubMed: 9593887]

91. Jin ZQ, Zhou HZ, Cecchini G, Gray MO, Karliner JS. MnSOD in mouse heart: acute responses to ischemic preconditioning and ischemia-reperfusion injury. Am. J. Physiol. Heart Circ. Physiol. 2005; 288:H2986–H2994. [PubMed: 15681709]

92. Hsu JL, Hsieh Y, Tu C, O'Connor D, Nick HS, Silverman DN. Catalytic properties of human manganese superoxide dismutase. J. Biol. Chem. 1996; 271:17687–17691. [PubMed: 8663465]

93. Shinkarev VP, Wraight CA. Intermonomer electron transfer in the bc1 complex dimer is controlled by the energized state and by impaired electron transfer between low and high potential hemes. FEBS Lett. 2007; 581:1535–1541. [PubMed: 17399709]

94. Crofts AR, Shinkarev VP, Kolling DR, Hong S. The modified Q-cycle explains the apparent mismatch between the kinetics of reduction of cytochromes c1 and bH in the bc1 complex. J Biol Chem. 2003; 278:36191–36201. [PubMed: 12829696]

95. Bielski BH, Cabelli DE. Highlights of current research involving superoxide and perhydroxyl radicals in aqueous solutions. Int. J. Radiat. Biol. 1991; 59:291–319. [PubMed: 1671684]

96. Butler J, Jayson GG, Swallow AJ. The reaction between the superoxide anion radical and cytochrome c. Biochim. Biophys. Acta. 1975; 408:215–222. [PubMed: 60]

97. Butler J, Koppenol WH, Margoliash E. Kinetics and mechanism of the reduction of ferricytochrome c by the superoxide anion. J. Biol. Chem. 1982; 257:10747–10750. [PubMed: 6286671]

98. Covian R, Trumpower BL. The dimeric structure of the cytochrome bc(1) complex prevents center P inhibition by reverse reactions at center N. Biochim. Biophys. Acta. 2008; 1777:1044–1052. [PubMed: 18454936]

99. Engstrom G, Rajagukguk R, Saunders AJ, Patel CN, Rajagukguk S, Merbitz-Zahradnik T, Xiao K, Pielak GJ, Trumpower B, Yu CA, Yu L, Durham B, Millett F. Design of a ruthenium-labeled cytochrome c derivative to study electron transfer with the cytochrome bc1 complex. Biochemistry. 2003; 42:2816–2824. [PubMed: 12627947]

100. Millett F, Durham B. Kinetics of Electron Transfer within Cytochrome bc (1) and Between Cytochrome bc (1) and Cytochrome c. Photosynth. Res. 2004; 82:1–16. [PubMed: 16228609]

101. Jones DP. Intracellular diffusion gradients of O2 and ATP. Am. J. Physiol. 1986; 250:C663–C675. [PubMed: 3010727]

102. Vinogradov AD. NADH/NAD+ interaction with NADH: ubiquinone oxidoreductase (complex I). Biochim. Biophys. Acta. 1998; 1364:169–185. [PubMed: 9593879]

103. Lambert AJ, Buckingham JA, Boysen HM, Brand MD. Low complex I content explains the low hydrogen peroxide production rate of heart mitochondria from the long-lived pigeon, Columba livia. Aging Cell. 2010; 9:78–91. [PubMed: 19968628]

Highlights

- Computational model of ROS production by the respiratory chain was developed.
- Semiquinone of Complex I should be considered to be an additional ROS forming site.
- Inhibition of Complexes III, IV reduces ROS production by Complex I semiquinone.
- Reduced iron-sulfur protein leaves the cyt *b* position only after cyt b_H reduction.
- Depolarization activates ROS production by antimycin-inhibited Complex III.

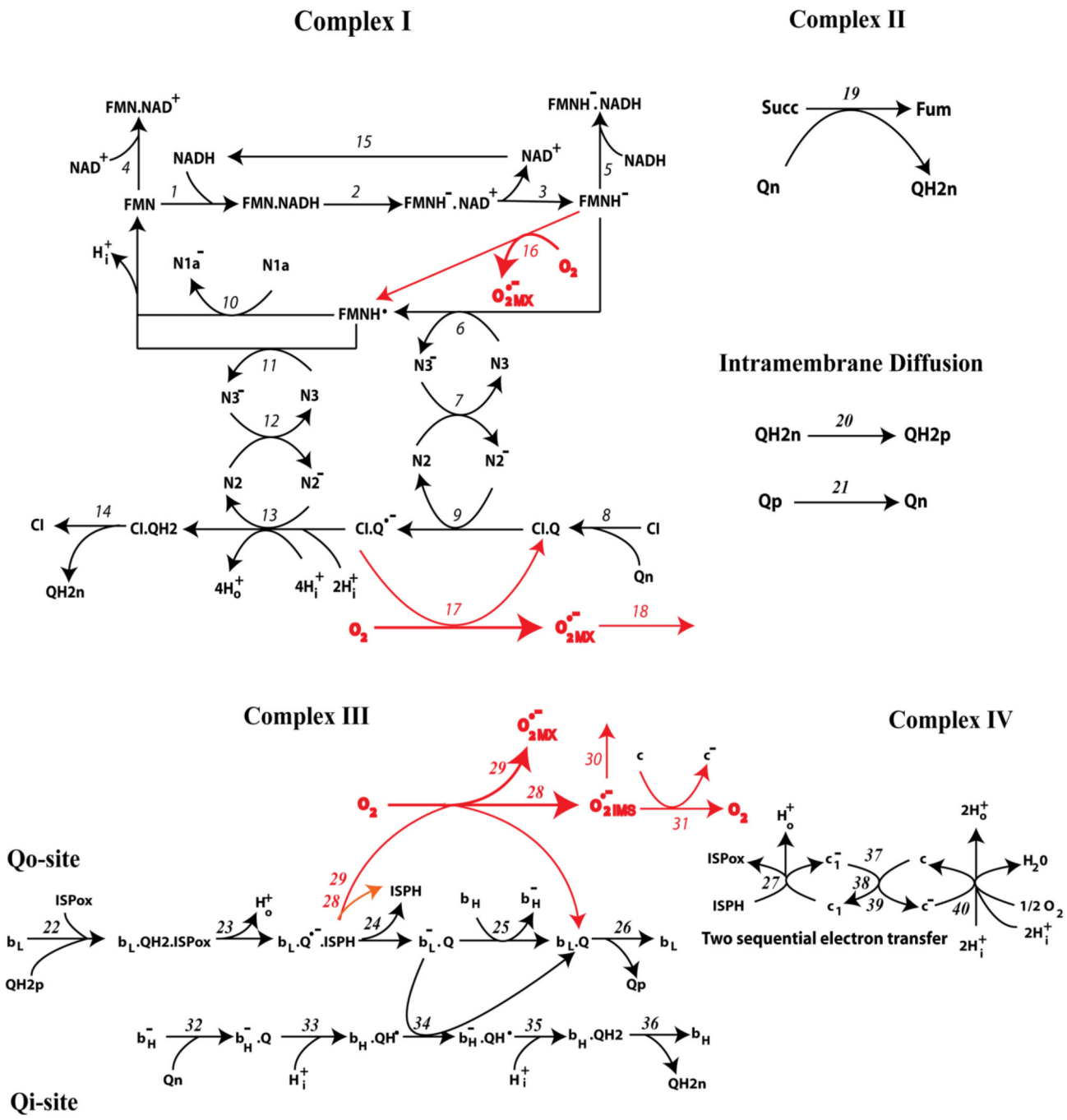

Fig. 1. Kinetic scheme of electron transfer and superoxide $O_2^{\bullet-}$ production in the respiratory chain with early dissociation of ISPH in complex III

Dissociation of ISPH from cyt b_L occurs in reaction (24). Reactions of $O_2^{\bullet-}$ formation and utilization are shown by red arrows. The detailed reaction network is presented in Table 1.

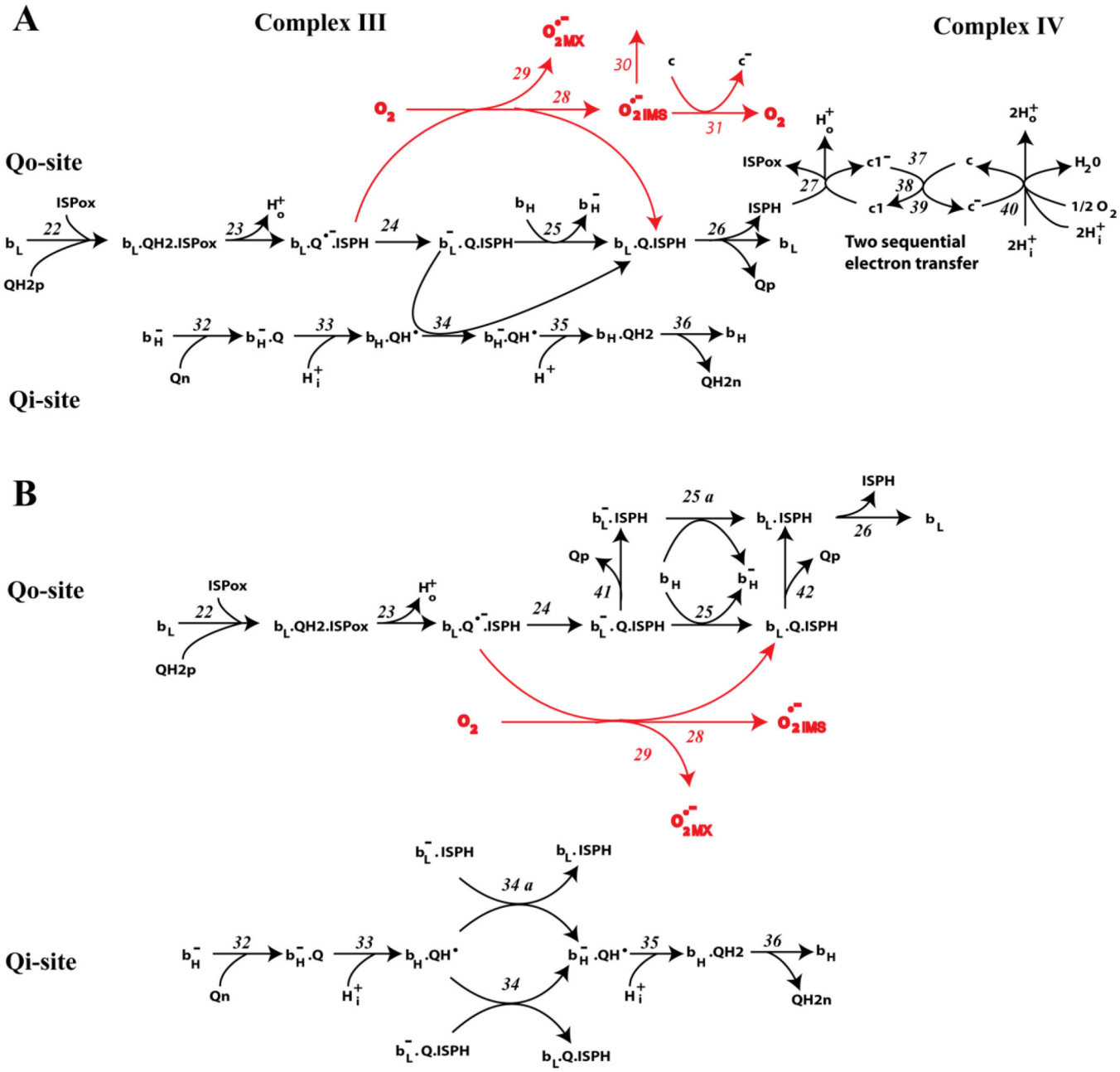

Fig. 2. Kinetic schemes of electron transfer and $O_2^{\cdot-}$ production in complex III with late dissociation of ISPH

(A) All reactions are the same as in Fig. 1 except reactions (24) and (26). Dissociation of ISPH from the Qo site (reaction (26)) occurs later than in Fig. 1 in which ISPH dissociates during reaction (24). **(B)** Kinetic scheme of electron transfer with late dissociation of ISPH and additionally with binding of oxidized Q to the Qo site when cyt b_L is reduced (reaction (41). All reactions are the same as in Fig. 2A except reactions (25), (25a), (26), (34a), (41), and (42).

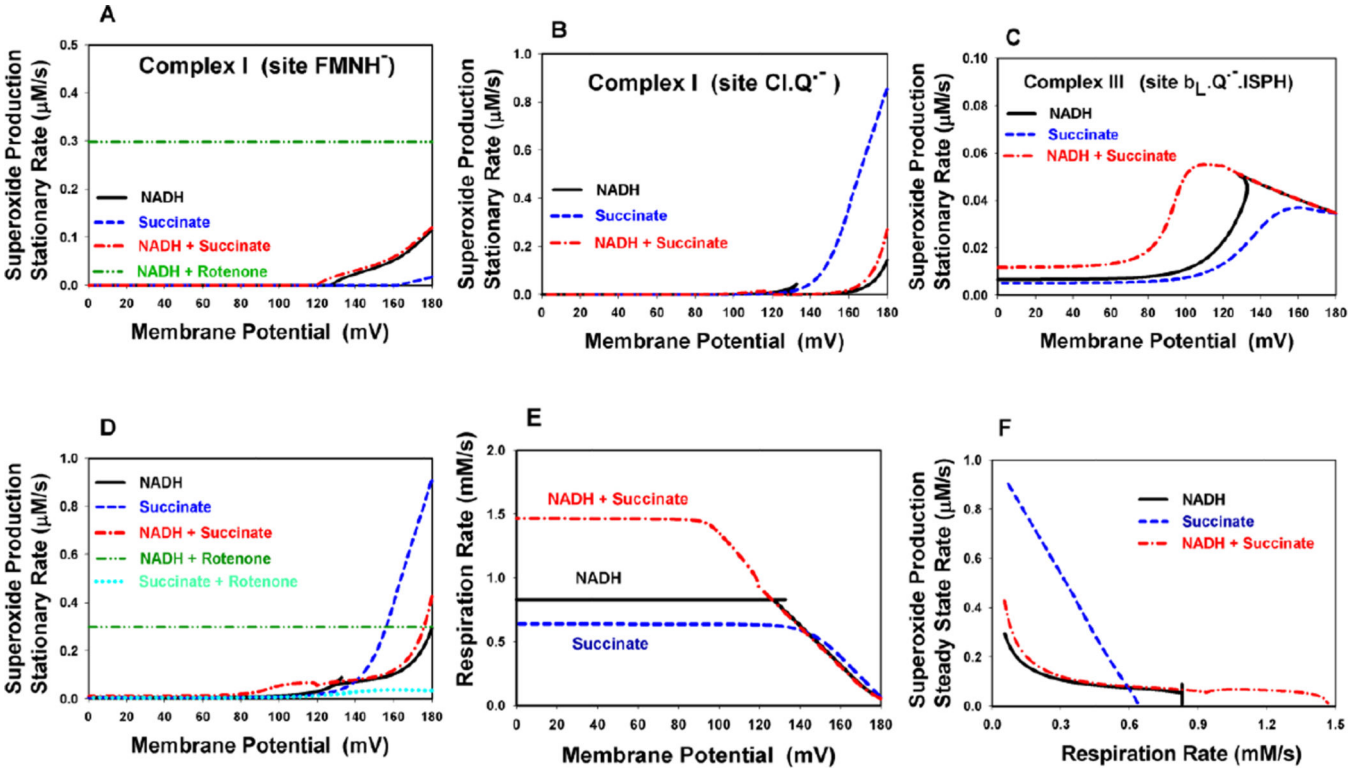

Fig. 3. Computer simulated stationary rate of respiration and $O_2^{\cdot-}$ production at different membrane potential in the presence of different respiratory substrates

(A–C)) The rate of $O_2^{\cdot-}$ generation by different sites of Complexes I and III: (**A**) site $FMNH^-$ of Complex I; (**B**) the semiquinone of Complex I (site $CI.Q^{\cdot-}$); (**C**) the unstable semiquinone of Complex III (site $b_L.Q^{\cdot-}$.ISPH). (**D**) The total rate of $O_2^{\cdot-}$ production by Complexes I and III. (**E**) The respiration rate. (**F**) The relationship between the rates of respiration and total $O_2^{\cdot-}$ production by the entire respiratory chain when using different respiratory substrates. Computer simulation was carried out with the mathematical model at kinetic parameter values presented in Table 2. Different curves correspond to different respiratory substrates ± rotenone: black solid curve – NADH alone; blue dashed curve – succinate alone; red dash-dot curve – NADH + succinate; dark green dash-dot-dot curve – NADH + rotenone; cyan dotted curve – succinate + rotenone. Designation for every curve is also shown in the Figure. Different respiratory substrates correspond to the following parameter values: NADH alone -V_{max19} = 0, k_{15} = 0.45 s^{-1}; succinate alone - V_{max19} = 4270 μM/s; k_{15} = 0; NADH+succinate - V_{max19} = 4270 μM/s; k_{15} = 0.45 s^{-1}. In order to simulate the effect of rotenone, we suggested that $v_8 = v_{14} = 0$ in the computational model.

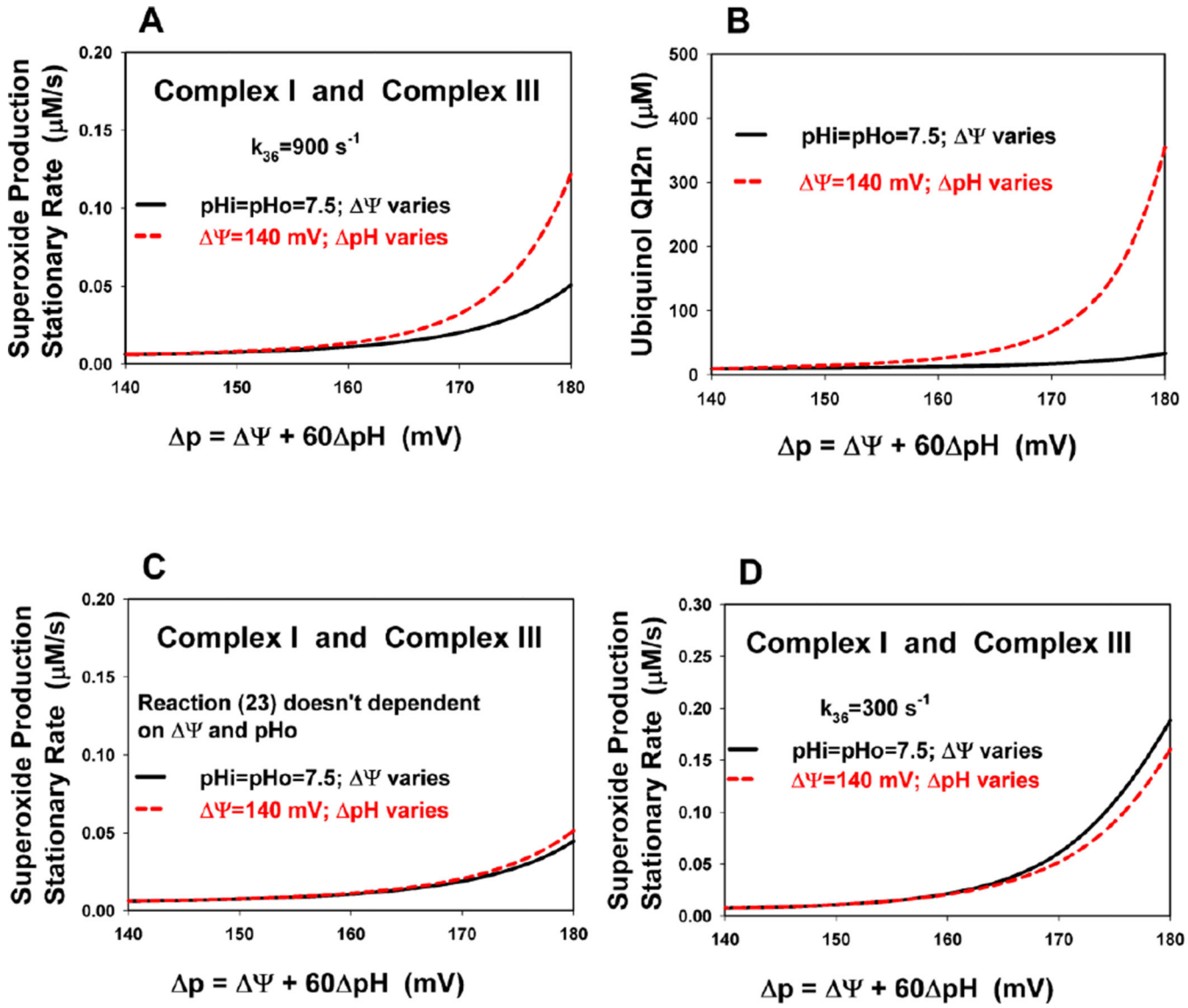

Fig. 4. Computer simulation of the stationary $O_2^{\cdot-}$ production rate and ubiquinol QH2n concentration at different values of proton motive force (expressed in mV) in the presence of succinate alone

(**A**) Solid black curves present changes in the total $O_2^{\cdot-}$ production rate by Complexes I and III at different values of membrane potential (ΔΨ) and ΔpH = 0 (pHi = pHo = 7.5). Dashed red curves present the total $O_2^{\cdot-}$ production rate at different values of ΔpH and ΔΨ=140 mV. Variation in ΔpH was made by introducing changes in pHo at constant pHi = 7.5. All parameter values are the same as for Fig. 3 except the rate constant of QH_2 release in Qi site, k_{36} = 900 s^{-1}. (**B**) Solid black and dashed red curves show ubiquinol concentration at the negative side of the membrane (QH_{2n}) for the same conditions as for (A). (**C**) Simulation of the $O_2^{\cdot-}$ production rate for the same conditions as for (A) except for the equilibrium constant of reaction (23) in Table 1, where exp(F · δ_1 · ΔΨ/R · T + 2.3 · (7 – pHo)) was taken as 1 to make reaction (23) independent of ΔΨ and pHo. (**D**) Simulated $O_2^{\cdot-}$ production rate

for the same conditions as for (A) except for the rate constant k_{36}, which was decreased from 900 to 300 s^{-1}.

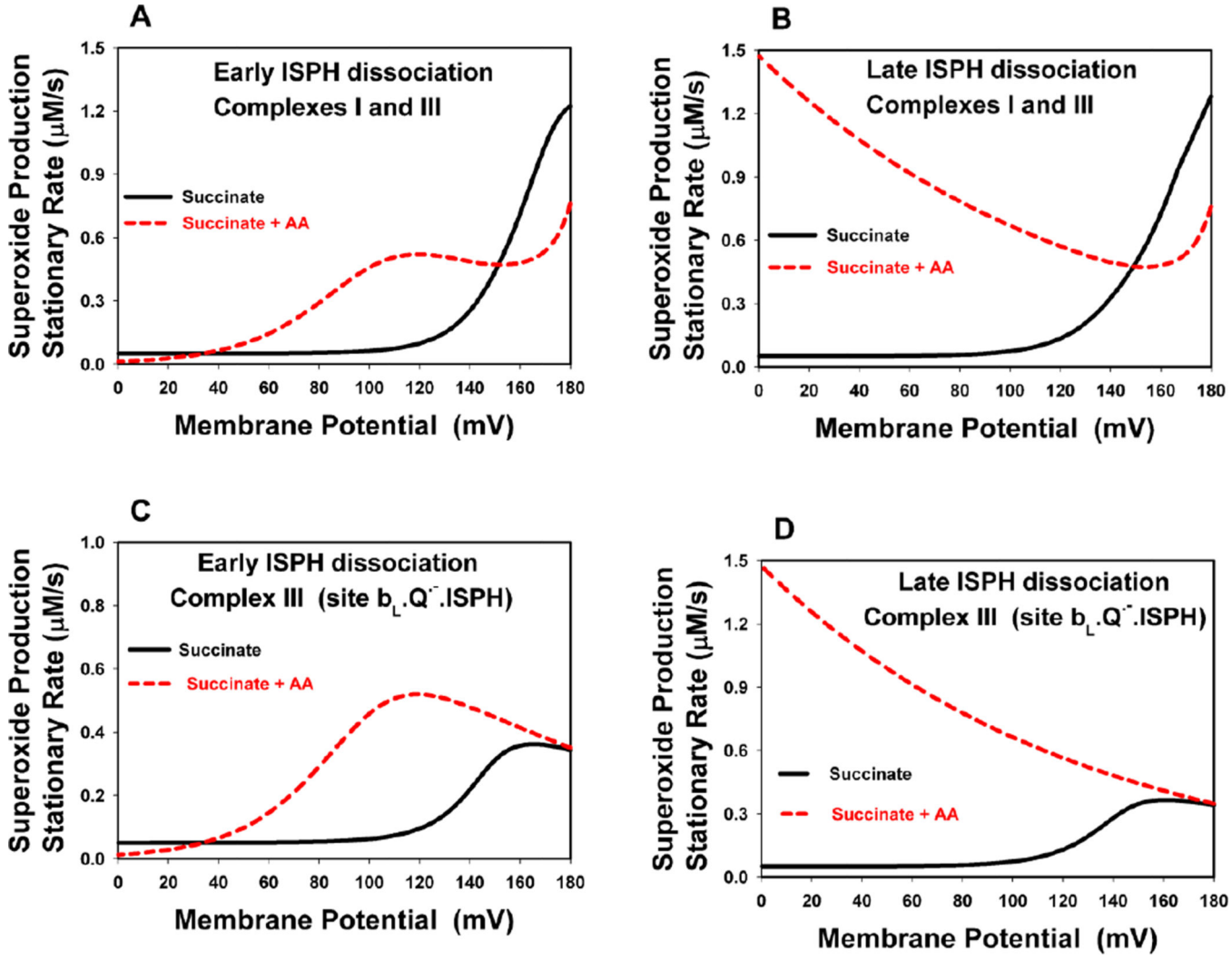

Fig. 5. Computer simulated effect of Antimycin A on the $O_2^{\cdot-}$ production rate

(**A, B**) The total computer simulated superoxide production rate by Complexes I and III in models E (A) and L (B). (**C, D**) The rate of $O_2^{\cdot-}$ generation by the unstable semiquinone of Complex III in models E (C) and L (D). Action of AA was simulated in the models by taking v_{34} equal 0 (see text for detail). Values of all parameters in the models without AA are the same as for Fig. 3 except k_{28} and k_{29} which equal 20 $\mu M^{-1}s^{-1}$. δ_1 = 0.2 in both E and L models. Black solid curves correspond to the computer simulated $O_2^{\cdot-}$ production rate in the control models and red dashed curves are the $O_2^{\cdot-}$ production rates in the same models except for the rate v_{34} which was taken to be 0 to simulate the effect AA. Succinate alone was modeled as a respiratory substrate (V_{max19}=4270 μM/s; k_{15}=0)

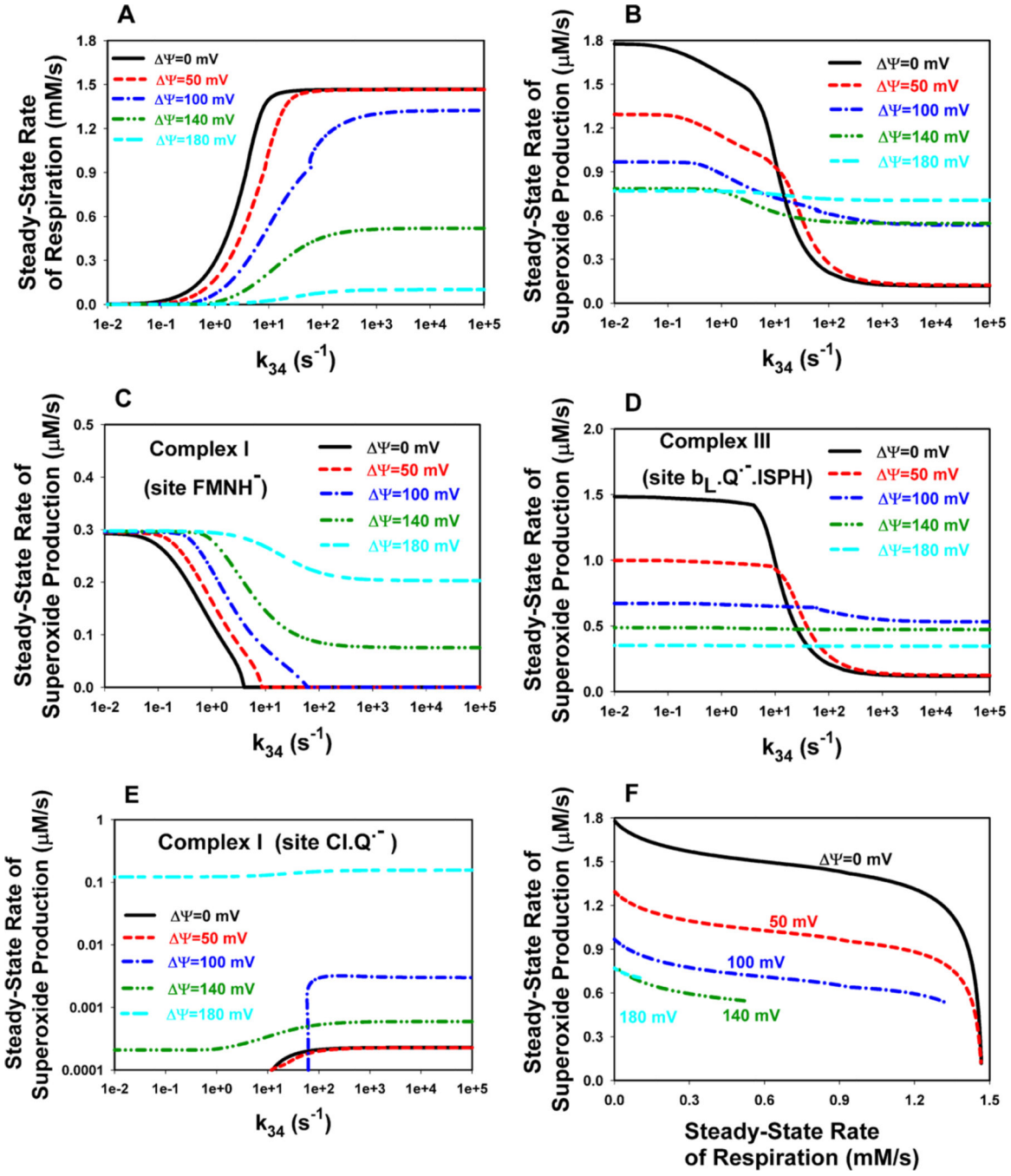

Fig. 6. Computer simulated partial inhibition of the $O_2^{\cdot-}$ production rate by antimycin A

(**A**–E) Steady state dependency of the rates of respiration (A), total $O_2^{\cdot-}$ production by Complexes I and III (B), $O_2^{\cdot-}$ production by the reduced flavin of Complex I (C), the unstable semiquinone of Complex III (D), and the semiquinone of Complex I (E) on the rate constant k_{34} at different values of ΔΨ.

Relationship between rates of respiration and total $O_2^{\cdot-}$ production (F) represents values of the rates from (A) and (B). Black solid curves correspond to the computer simulated rates at ΔΨ = 0; red dashed curves – ΔΨ = 50 mV; blue dash-dot curve −ΔΨ = 100 mV; dark green

dash-dot-dot curve – $\Delta\Psi$ = 140 mV; cyan long-short-short dash – $\Delta\Psi$ = 180 mV. All results were performed using the model L with NADH + succinate as respiratory substrates. All parameter values are the same as for Fig. 5. V_{max19} = 4270 μM/s; k_{15} = 0.45 s^{-1}.

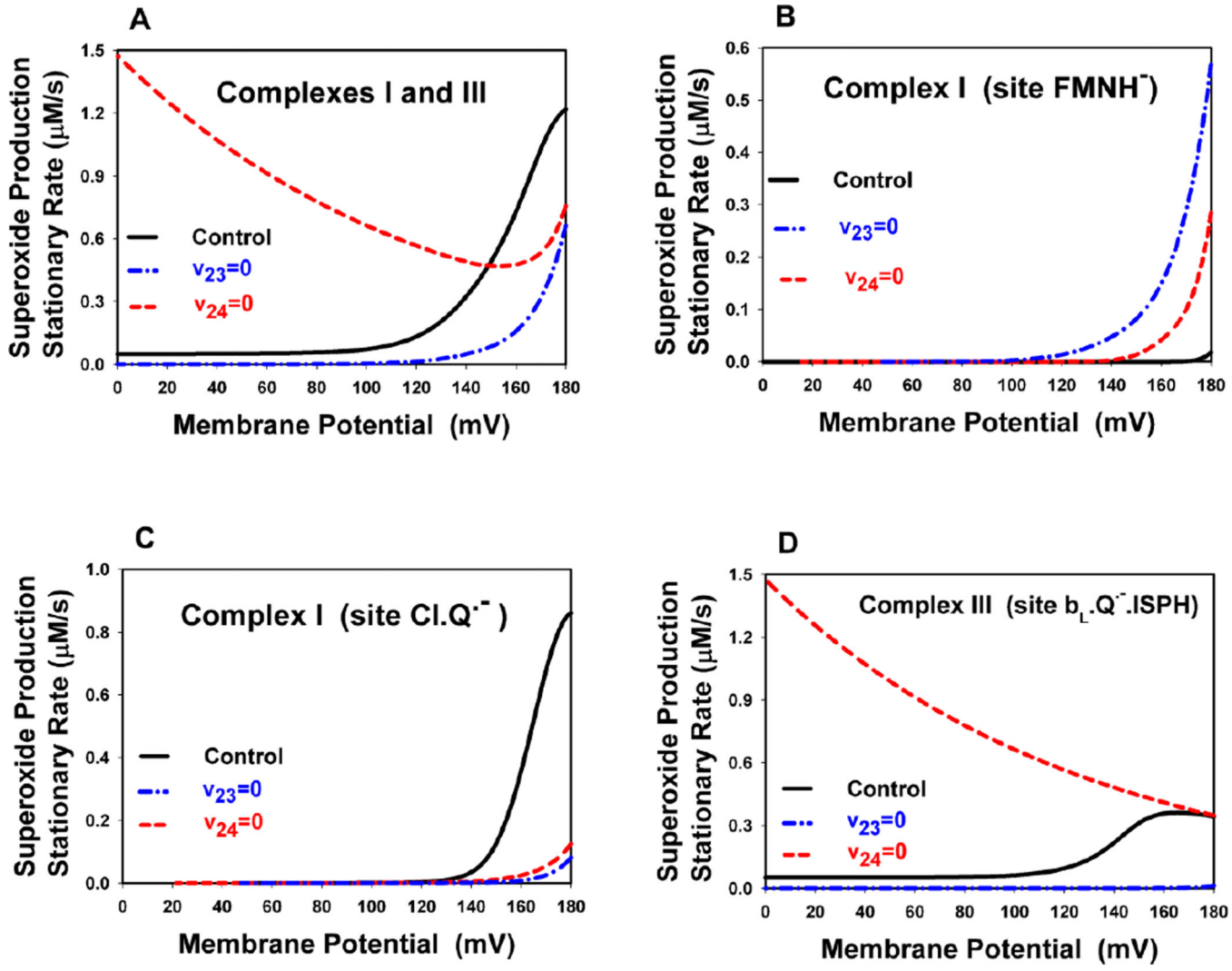

Fig. 7. Computer simulated effect of inhibition of different reactions at the Qo site on the $O_2^{\cdot-}$ production rate during oxidation of succinate alone

(A–D) The computer simulated $O_2^{\cdot-}$ production rate upon inhibition of the first (v_{23}=0) or the second (v_{24}=0) electron transfer in the Qo site of Complex III. (**A**) The total rate of $O_2^{\cdot-}$ generation by both Complexes I and III. **(B–D)** The rate of $O_2^{\cdot-}$ generation by different sites of Complexes I and III: (**B**) the site $FMNH^-$ of Complex I; (**C**) the semiquinone of Complex I (complex $CI.Q^{\cdot-}$); (**D**) the unstable semiquinone of Complex III (complex $b_L.Q^{\cdot-}$.ISPH). All computer simulations were performed using model E. Values of all parameters in the control model E are the same as for Fig. 5. Black solid curves correspond to the computer simulated $O_2^{\cdot-}$ production rate in the control model E. Blue dash-dot and red dashed curves are the $O_2^{\cdot-}$ production rates in the same model E, except for the rates v_{23} and v_{24} which were taken to be 0 to simulate the effects of stigmatellin or myxothiazol. Succinate alone was modeled as a respiratory substrate (V_{max19} = 4270 μM/s; k_{15} = 0).

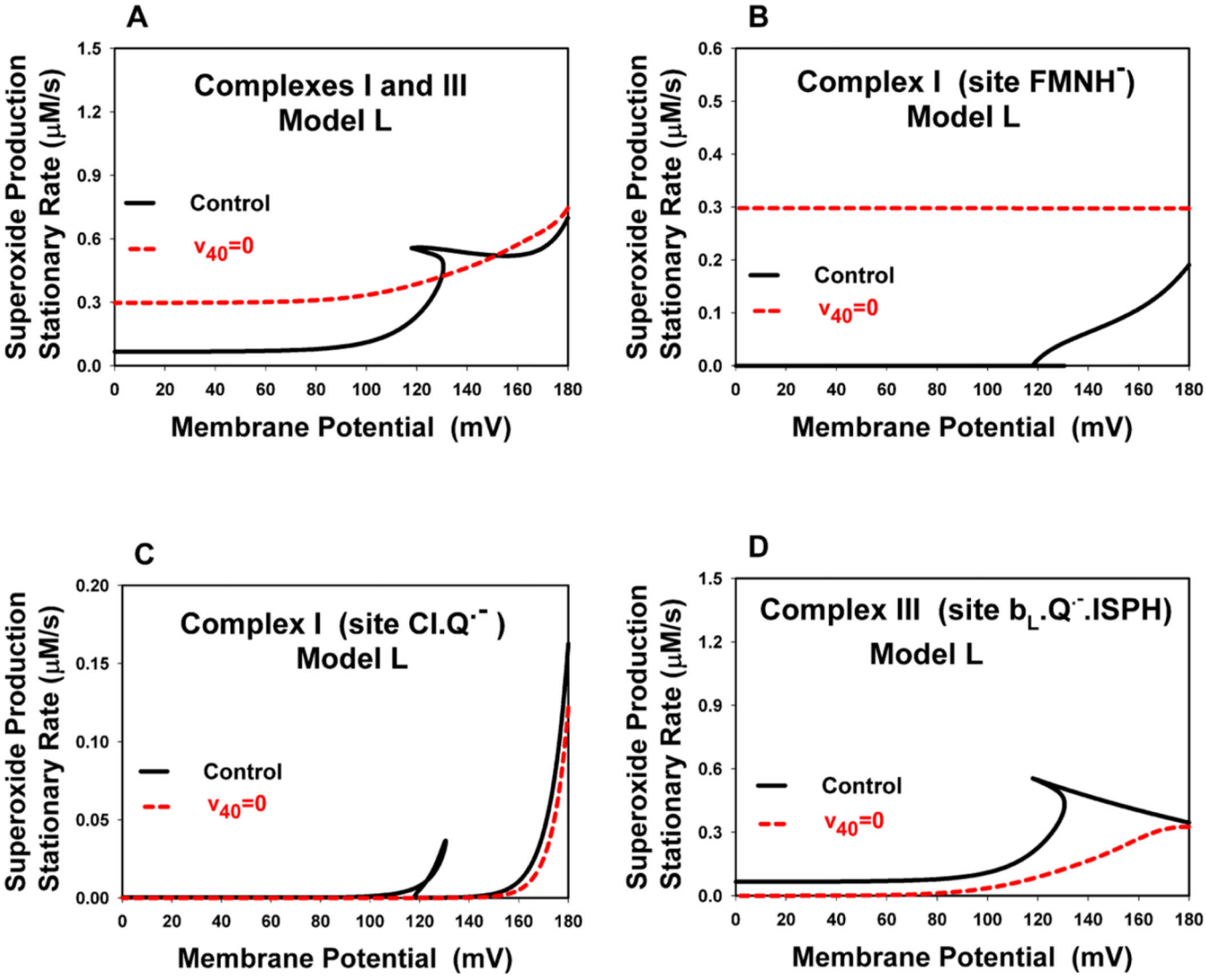

Fig. 8. Computer simulated effect of inhibition of cytochrome *c* oxidase on the $O_2^{\cdot-}$ production rate during NADH oxidation

(A–D) The computer simulated $O_2^{\cdot-}$ production rate at inhibition of cytochrome c oxidase (v_{40}=0). NADH alone was simulated as substrate of respiration. (**A**) The total rate of $O_2^{\cdot-}$ generation by both Complexes I and III. **(B–D)** The rate of $O_2^{\cdot-}$ generation by different sites of Complexes I and III: (**B**) the site $FMNH^-$ of Complex I; (**C**) the semiquinone of Complex I (complex $CI.Q^{\cdot-}$); (**D**) the unstable semiquinone of Complex III (complex $b_L.Q^{\cdot-}$.ISPH). All computer simulations were performed using model L. Values of all parameters are the same as for Fig. 5. Black solid curves correspond to the computer simulated $O_2^{\cdot-}$ production rate in the control model L and red dashed curves are the $O_2^{\cdot-}$ production rates in the same model L except the rate v_{40} which was taken 0 to simulate the effect of inhibition of cytochrome c oxidase. Succinate alone was modeled as a respiratory substrate (V_{max19} = 4270 μM/s; k_{15} = 0).

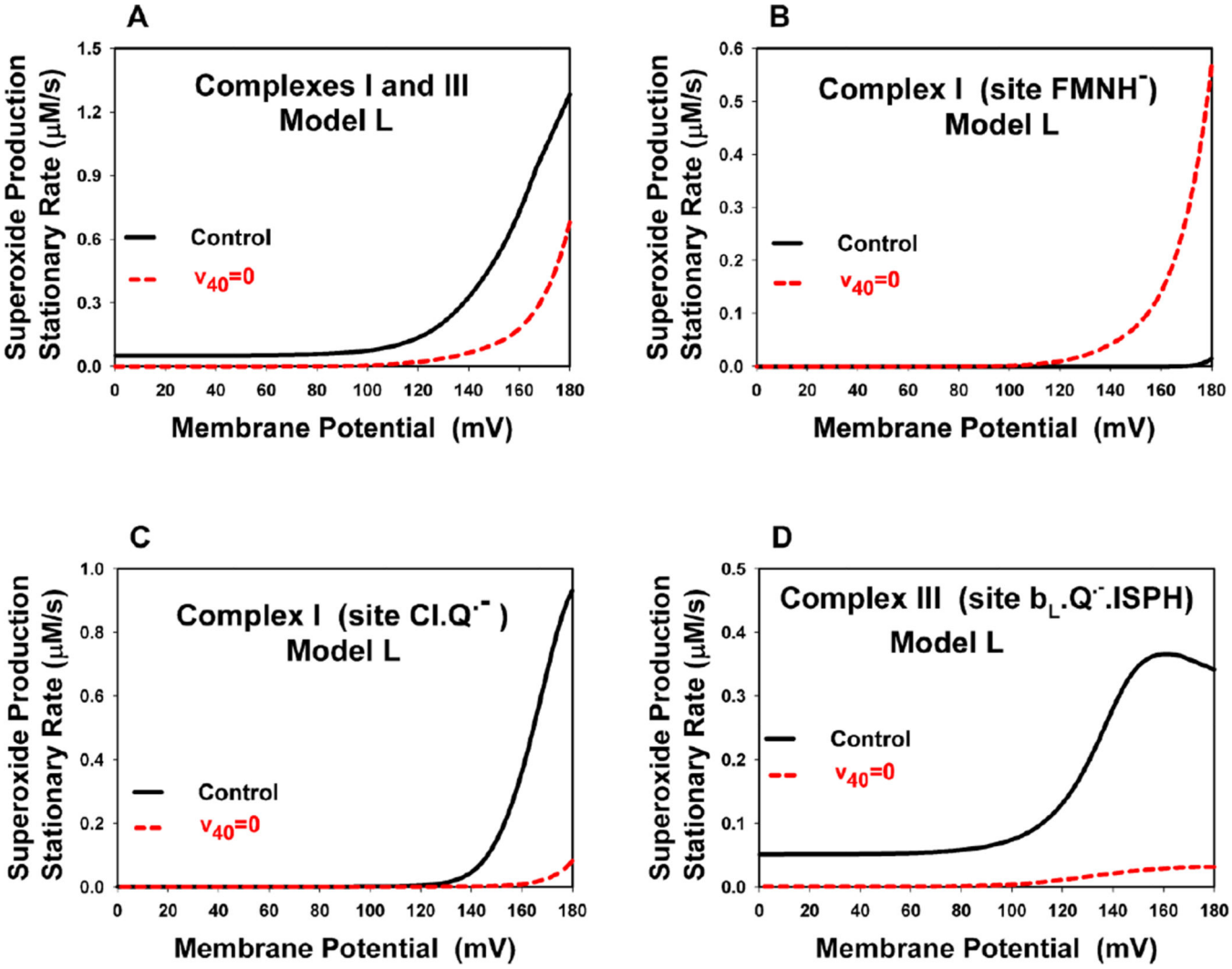

Fig. 9. Computer simulated effect of inhibition of cytochrome c oxidase on the $O_2^{\cdot-}$ production rate during succinate oxidation

(A–D) The computer simulated $O_2^{\cdot-}$ production rate upon inhibition of cytochrome c oxidase (v_{40}=0). Succinate alone was simulated as substrate of respiration. (**A**) The total rate of $O_2^{\cdot-}$ generation by both Complexes I and III. **(B–D)** The rate of $O_2^{\cdot-}$ generation by different sites of Complexes I and III: (**B**) the site $FMNH^-$ of Complex I; (**C**) the semiquinone of Complex I (complex $CI.Q^{\cdot-}$); (**D**) the unstable semiquinone of Complex III (complex $b_L.Q^{\cdot-}$.ISPH). All the computer simulations were performed using the model L. Values of all parameters are the same as for Fig. 5. Black solid curves correspond to the computer simulated ROS production rate in the control model L and red dashed curves are the $O_2^{\cdot-}$ production rates in the same model L except rate v_{40}, which was taken to be 0 to simulate the effect of inhibition of cytochrome c oxidase. Succinate alone was modeled as a respiratory substrate (V_{max19} = 4270 μM/s; k_{15} = 0)

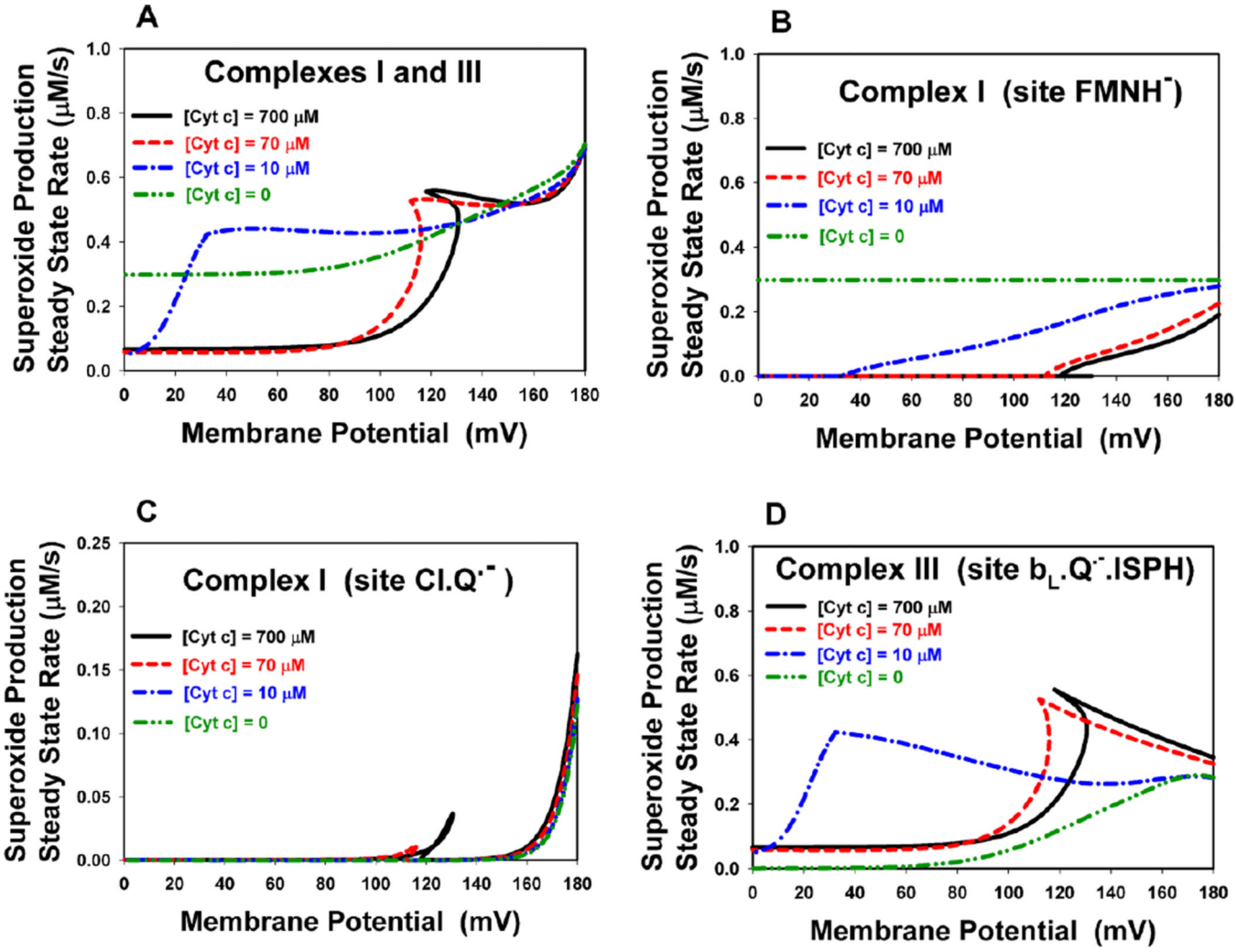

Fig. 10. Computer simulated effect of cytochrome *c* depletion on the $O_2^{\cdot-}$ production rate during NADH alone oxidation

(A–D) The computer simulated $O_2^{\cdot-}$ production rate at different cyt c concentration, [Cyt c]. NADH alone was simulated as substrate of respiration. (**A**) The total rate of $O_2^{\cdot-}$ generation by both Complexes I and III. **(B–D)** The rate of $O_2^{\cdot-}$ generation by different sites of Complexes I and III: (**B**) the site FMNH$^-$ of Complex I; (**C**) the semiquinone of Complex I (complex CI.Q$^{\cdot-}$); (**D**) the unstable semiquinone of Complex III (complex b_L.Q$^{\cdot-}$.ISPH). All computer simulations were performed using model L. Values of all parameters are the same as for Fig. 5. Black solid curves corresponds to [Cyt *c*]=700 μM; red dashed curve - [Cyt *c*]=70 μM; blue dash-dot curve - [Cyt *c*]=10 μM; green dash-dot-dot - [Cyt *c*]= 0 μM. NADH alone was modeled as a respiratory substrate (V_{max19}=0; k_{15}=0.45 s^{-1})

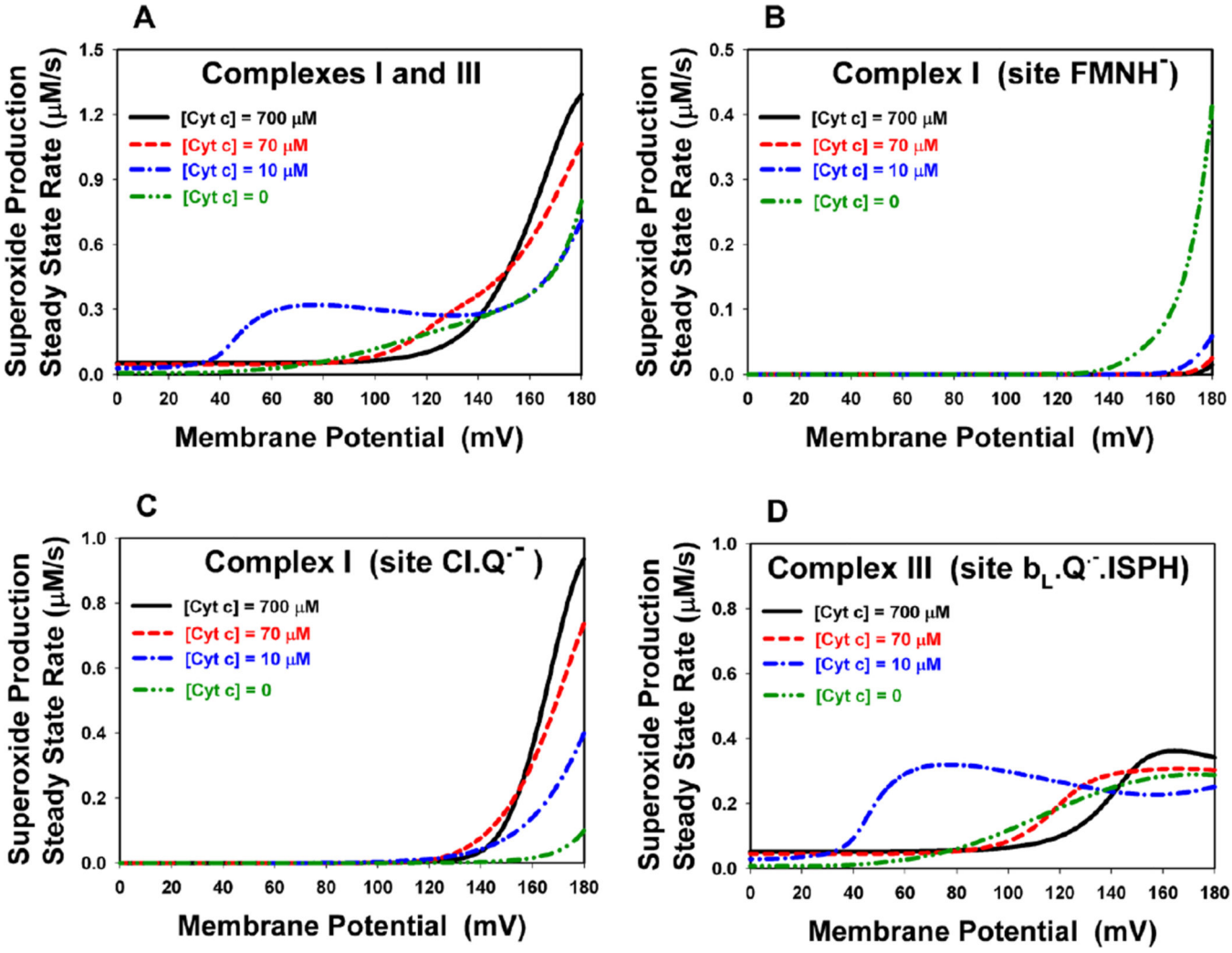

Fig. 11. Computer simulated effect of cytochrome c depletion on the $O_2^{\cdot-}$ production rate during oxidation of succinate alone

(A–D) The computer simulated $O_2^{\cdot-}$ production rate at different cyt c concentration, [Cyt c]. Succinate alone was simulated as substrate of respiration. (**A**) The total rate of $O_2^{\cdot-}$ generation by both Complexes I and III. **(B–D)** The rate of $O_2^{\cdot-}$ generation by different sites of Complexes I and III: (**B**) the site $FMNH^-$ of Complex I; (**C**) the semiquinone of Complex I (complex $CI.Q^{\cdot-}$); (**D**) the unstable semiquinone of Complex III (complex $b_L.Q^{\cdot-}$.ISPH). All the computer simulations were performed using model L. Values of all parameters are the same as for Fig. 5. Black solid curves corresponds to [Cyt *c*]=700 μM; red dashed curve - [Cyt *c*]=70 μM; blue dash-dot curve - [Cyt *c*]=10 μM; green dash-dot-dot - [Cyt *c*]= 0 μM. Succinate alone was modeled as a respiratory substrate (V_{max19} = 4270 μM/s; k_{15} = 0)

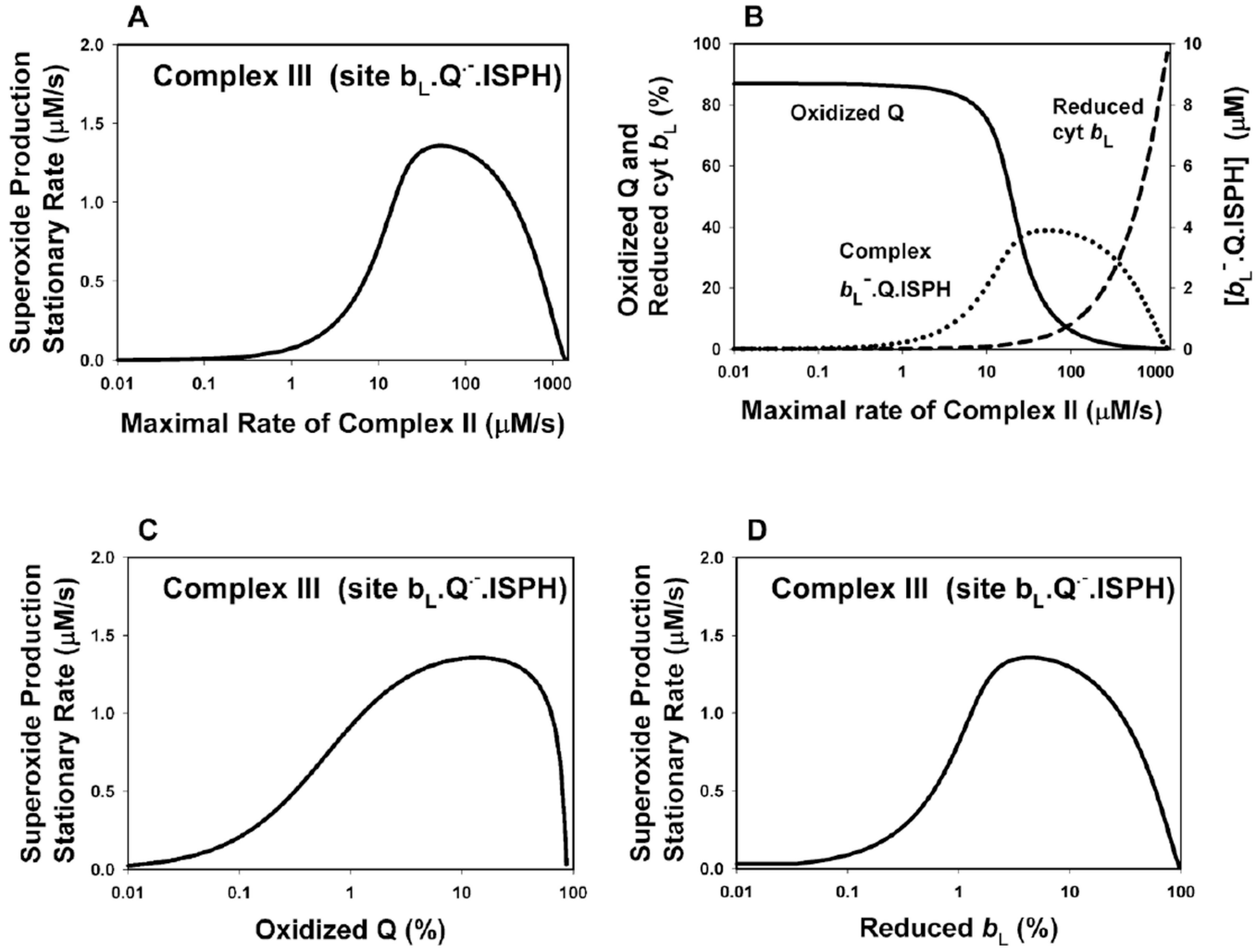

Fig. 12. Computer simulated $O_2^{\cdot-}$ production by antimycin-inhibited Complex III upon inhibition of succinate dehydrogenase during oxidation of succinate alone

(**A**) Dependence of the rate of $O_2^{\cdot-}$ production on the maximal rate (V_{max19}) of succinate dehydrogenase. (**B**) Dependence of the oxidized Q and reduced cyt b_L fractions as well as the concentration of the b_L.Q.ISPH complex on the maximal rate of succinate dehydrogenase. (**C**) Dependence of the rate of $O_2^{\cdot-}$ production on the oxidized Q fraction. (**D**) Dependence of the rate of $O_2^{\cdot-}$ production on the reduced cyt b_L fraction. The rates v_{34} and v_{34a} were taken to be 0 to simulate the effect AA. All the computer simulations were performed with the model according to the kinetic scheme presented in Fig. 2B under steady state conditions. Values of all parameters are the same as for Fig. 9 except $k_{26} = 1{\cdot}10^4\ s^{-1}$; $K_{eq26} = 1{\cdot}10^3$ μM; $k_{32} = 1.7\ \mu M^{-1}{\cdot}s^{-1}$; $k_{41} = k_{42} = 1{\cdot}10^5\ s^{-1}$; $K_{eq41} = K_{eq42} = 1{\cdot}10^3$ μM; $k_{25a} = k_{34a} = 1{\cdot}10^5\ s^{-1}$; $K_{eq25a} = K_{eq34a} = 40$; $\Delta\Psi = 0$. The oxidized Q fraction was calculated as $100\% \cdot ([Qn] + [Qp] + [b_L^-.Q.ISPH] + [b_L.Q.ISPH])/[Q_{tot}]$ and reduced cyt b_L fraction as $100\% \cdot ([b_L^-.Q.ISPH] + [b_L^-.ISPH])/[b_{Ltot}]$.

Table 1

Reactions and rate equations in the model of respiratory chain.

No	Reaction	Rate equation
Electron transfer in Complex I		
1	NADH + FMN = FMN.NADH	$V_1=k_1 \cdot (NADH \cdot FMN – FMN.NADH/K_{eq1})$
2	FMN.NADH = $FMNH^{-}.NAD^{+}$	$V_2=k_2 \cdot (FMN.NADH - FMNH^{-}.NAD^{+}/K_{eq2})$
3	$FMNH^{-}.NAD^{+} = FMNH^{-} + NAD^{+}$	$V_3=k_3 \cdot (FMNH^{-}.NAD^{+} - FMNH^{-} \cdot NAD^{+}/K_{eq3})$
4	$FMN + NAD^{+} = FMN.NAD^{+}$	$V_4=k4 \cdot (FMN \cdot NAD^{+} - FMN.NAD^{+}/K_{eq4})$
5	$FMNH^{-} + NADH = FMNH^{-}.NADH$	$V_5=k_5 \cdot (FMNH^{-} \cdot NADH - FMNH^{-}.NADH/K_{eq5})$
The first electron transfer		
6	$FMNH^{-} + N3 = FMNH^{\cdot} + N3^{-}$	$V_6=k_6 \cdot (FMNH^{-} \cdot N3 – FMNH^{\cdot} \cdot N3^{-}/ K_{eq6})$
7	$N3^{-} + N2 = N3 + N2^{-}$	$V_7=k_7 \cdot (N3^{-} \cdot N2 - N3 \cdot N2^{-}/ K_{eq7})$
8	CI + Qn = CI.Q	$V_8=k_8 \cdot (CI \cdot Qn - CI.Q/ K_{eq8})$
9	$CI.Q + N2^{-} = CI.Q^{\cdot-} + N2$	$V_9=k_9 \cdot (CI.Q - CI.Q^{\cdot-} /K_{eq9})$
The second electron transfer		
10[a]	$FMNH^{\cdot} + N1a = FMN + N1a^{-} + Hi^{+}$	$V_{10}=k_{10} \cdot (FMNH^{\cdot} \cdot N1a – FMN \cdot N1a^{-} \cdot \exp(2.3 \cdot (7-pHi)) / K_{eq10})$
11[a]	$FMNH^{\cdot} + N3 = FMN + N3^{-} + Hi^{+}$	$V_{11}=k_{11} \cdot (FMNH^{\cdot} \cdot N3 – FMN \cdot N3^{-} \cdot \exp(2.3 \cdot (7-pHi)) / K_{eq11})$
12	$N2 + N3^{-} = N2^{-} + N3$	$V_{12}=k_{12} \cdot (N2 \cdot N3^{-} - N2^{-} \cdot N3/ K_{eq12})$
13[a]	$N2^{-} + CI.Q^{\cdot-} + 8 \cdot Hi^{+} = N2 + CI.QH2 + 6 \cdot Ho^{+}$	$V_{13}=k_{13} \cdot (N2^{-} \cdot CI.Q^{\cdot-} \cdot \exp(2 \cdot 2.3 \cdot (7-pHi)) - N2 \cdot CI.QH2 \cdot \exp(4 \cdot (F \cdot \Delta\Psi/R \cdot T + 2.3 \cdot (pHi – pHo)))/K_{eq13})$
14	CI.QH2 = CI + QH2n	$V_{14}=k_{14} \cdot (CI.QH2 – CI \cdot QH2n/K_{eq14})$
NAD^{+} reduction to NADH in mitochondrial matrix		
15	$NAD^{+} = NADH$	$V_{15}=k_{15} \cdot (NAD^{+} - NADH/K_{eq15})$
	Superoxide anion ($O_2^{\cdot-}{}_{mx}$) production by Complex I into the mitochondrial matrix	
16	$FMNH^{-} + O_2 = FMNH^{\cdot} + O_2^{\cdot-}{}_{mx}$	$V_{16}=k_{16} \cdot (FMNH^{-} \cdot O_2 - FMNH^{\cdot} \cdot O_2^{\cdot-}{}_{mx} /K_{eq16})$
17	$CI.Q^{\cdot-} + O_2 = CI.Q + O_2^{\cdot-}{}_{mx}$	$V_{17}=k_{17} \cdot (CI.Q^{\cdot-} \cdot O_2 – CI.Q \cdot O_2^{\cdot-}{}_{mx} /K_{eq17})$
Superoxide anion dismutation in the mitochondrial matrix		
18	$2O_2^{\cdot-}{}_{mx} + 2Hi^{+} \rightarrow O_2 + H_2O_2$	$V_{18}=V_{max18} \cdot O_2^{\cdot-}{}_{mx}/(K_{m18} + O_2^{\cdot-}{}_{mx})$
Succinate dehydrogenase reaction (Complex II)		
19[b]	Succ + Qn → Fum +QH2n	$V_{19}=V_{max19} \cdot Qn/(Qn+QH2n)/(K_{19}+Qn/(Qn+QH2n))$
	Q and QH2 intramembrane diffusion	
20[c]	QH2n = QH2p	$V_{20}=k_{20} \cdot (QH2n - QH2p/K_{eq20})$
21[c]	Qp = Qn	$V_{21}=k_{21} \cdot (Qp - Qn/K_{eq21})$
Q_o–site reactions (Complex III)		
22	$b_L + ISPox + QH2p = b_L.QH2.ISPox$	$V_{22}=k_{22} \cdot (b_L \cdot ISPox \cdot QH2p - b_L.QH2.ISPox/K_{eq22})$
23[a]	$b_L.QH2.ISPox = b_L.Q^{\cdot-}.ISPH + Ho^{+}$	$V_{23}=k_{23} \cdot (b_L.QH2.ISPox - b_L.Q^{\cdot-}.ISPH \cdot \exp(F \cdot \delta_1 \cdot \Delta\Psi/R \cdot T + 2.3 \cdot (7 – pHo)) /K_{eq23})$

No	Reaction	Rate equation
24	$b_L.Q^{\cdot-}.ISPH = b_L^-.Q + ISPH$	$V_{24}=k_{24} \cdot (b_L.Q^{\cdot-}.ISPH - b_L^-.Q \cdot ISPH/K_{eq24})$
25[a]	$b_L^-.Q + b_H = b_L.Q + b_H^-$	$V_{25}=k_{25} \cdot (b_L^-.Q \cdot b_H^- - b_L.Q \cdot b_H^- \cdot \exp(F \cdot \delta_2 \cdot \Delta\Psi/R \cdot T)/K_{eq25})$
26	$b_L.Q = Q_p + b_L$	$V_{26}=k_{25} \cdot (bL.Q - Qp \cdot bL/K_{eq26})$
27[a]	$ISPH + c_1 = ISPox + c_1^- + Ho^+$	$V_{27}=k_{27} \cdot (ISPH \cdot c_1 – ISPox \cdot c_1^- \cdot \exp(2.3 \cdot (7 – pHo)) /K_{eq27})$
Superoxide anion ($O_2^{\cdot-}$$_{IMS}$) production by Complex III into the intermembrane space (IMS)		
28	$b_L.Q^{\cdot-}.ISPH + O_2 = b_L.Q + ISPH + O_2^{\cdot-}{}_{IMS}$	$V_{28}=k_{28} \cdot (b_L.Q^{\cdot-} .ISPH \cdot O_2 - b_L.Q \cdot ISPH \cdot O_2^{\cdot-}{}_{IMS} /K_{eq28})$
Superoxide anion ($O_2^{\cdot-}$$_{mx}$) production by Complex III into the mitochondrial matrix		
29	$b_L.Q^{\cdot-}.ISPH + O_2 = b_L.Q + ISPH + O_2^{\cdot-}{}_{mx}$	$V_{29}=k_{29} \cdot (b_L.Q^{\cdot-}.ISPH \cdot O_2 - b_L.Q \cdot ISPH \cdot O_2^{\cdot-}{}_{mx} /K_{eq29})$
Superoxide anion spontaneous dismutation and oxidation by cyt c in IMS		
30	$O_2^{\cdot-}{}_{IMS} + O_2^{\cdot-}{}_{IMS} \rightarrow$	$V_{30}=k_{30} \cdot (O_2^{\cdot-}{}_{IMS})^2$
31	$O_2^{\cdot-}{}_{IMS} + c = O_2 + c^-$	$V_{31}=k_{31} \cdot (O_2^{\cdot-}{}_{IMS} \cdot c – O_2 \cdot c^-/K_{eq31})$
Q_i–site reactions (Complex III)		
32	$b_H^- + Qn = b_H^-.Q$	$V_{32}=k_{32} \cdot (b_H^- \cdot Qn - b_H^-.Q/K_{eq32})$
33[a]	$b_H^-.Q + Hi^+ = b_H.QH^\cdot$	$V_{33}=k_{33} \cdot (b_H^-.Q - b_H.QH^\cdot \cdot \exp(F \cdot \delta_3 \cdot \Delta\Psi/R \cdot T - 2.3 \cdot (7 – pHi)) /K_{eq33})$
34[a]	$b_H.QH^\cdot + b_L^-.Q = b_H^-.QH^\cdot + b_L.Q$	$V_{34}=k_{34} \cdot (b_H.QH^\cdot \cdot b_L^-.Q - b_H^-.QH^\cdot \cdot b_L.Q \cdot \exp(F \cdot \delta_2 \cdot \Delta\Psi/R \cdot T)/K_{eq34})$
35[a]	$b_H^-.QH^\cdot + Hi^+ = b_H.QH2$	$V_{35}=k_{35} \cdot (b_H^-.QH^\cdot - b_H.QH2 \cdot \exp(F \cdot \delta_3 \cdot \Delta\Psi/R \cdot T - 2.3 \cdot (7 – pHi)) /K_{eq35})$
36	$b_H.QH2 = b_H + QH2n$	$V_{36}=k_{36} \cdot (b_H.QH2 - b_H \cdot QH2n/K_{eq36})$
Cytochrome c reduction		
37	$c_1^- + c = c_1^-.c$	$V_{37}=k_{37} \cdot (c_1^- \cdot c - c_1^-.c/K_{eq37})$
38	$c_1^-.c = c_1.c^-$	$V_{38}=k_{38} \cdot (c_1^-.c - c_1.c^-/K_{eq38})$
39	$c_1.c^- = c_1 + c^-$	$V_{39}=k_{39} \cdot (c_1.c^- - c_1 \cdot c^-/K_{eq39})$
Cytochrome c oxidase reaction (Complex IV)		
40[d]	$2 \cdot c^- + 4 \cdot Hi^+ + (1/2) \cdot O_2 = 2 \cdot c + H_2O + 2 \cdot Ho^+$	$V_{40} = k_{40} \cdot c^-/c_{tot}/(1 + k_{O2}/O_2) \cdot (\exp(-\Delta G^0/2 \cdot R \cdot T) \cdot \exp(2 \cdot 2.3 \cdot (7+pHo-2 \cdot pHi)) \cdot \exp(-\Delta\Psi \cdot F/R \cdot T) \cdot O_2^{0.25} \cdot c^- - c \cdot \exp(\Delta\Psi \cdot F/RT))$

[a] Reactions include steps dependent on membrane potential ($\Delta\Psi$) and/or inside (matrix) and/or outside (intermembrane space) H^+ concentration, pHi and pHo, respectively. The dependence of equilibrium constant (K_{eq}) of each of these reactions on $\Delta\Psi$ were described as $K_{eq}(\Delta\Psi) = K_{eq} \cdot \exp(n \cdot F \cdot \delta \cdot \Delta\Psi/R \cdot T)$, where K_{eq} is K_{eq} at $\Delta\Psi=0$, n is number of electrons or H^+ transferred through a part of the membrane δ. Other constants F, R, and T have usual meaning. The dependence of equilibrium constants on pH were described as in [21]: $K_{eq}(pH) = K_{eq} \cdot \exp(2.3 \cdot (7 – pH))$, where K_{eq} is K_{eq} at pH = 7.

[b] Rate equation was taken from experimental observations [88].

[c] Diffusion process was described as in the paper [21].

[d] Rate equation was taken from the theoretical work [26].

Biochim Biophys Acta. Author manuscript; available in PMC 2016 June 01.

Table 2

Parameter values for the model.

Reaction No	Midpoint potential E_m=E, (mV)	Equilibrium constant K_{eq}	$k_{forward}$	Other parameters	Reference
Electron transfer in Complex I					
1		0.01 μM^{-1}	83 $\mu M^{-1}\cdot s^{-1}$		[33, 34]*b* [34]*c*
2		0.032*d*	$1.44\cdot10^{12}\cdot s^{-1}$		[35]*c*
3		25 μM	10^6 s^{-1}		[33, 34] *b*
4		0.001 μM^{-1}	1 $\mu M^{1}\cdot s^{1}$		[33, 34] *b*
5		0.02 μM^{-1}	2 $\mu M^{-1}\cdot s^{-1}$		[33, 34]*b*
The first electron transfer					
6	$E(FMNH^{\cdot}/FMNH^{-})$ = −293 E(N3) = −250	5.6	$5\cdot10^8$ $\mu M^{-1}\cdot s^{-1}$	pH = 7	[89]*a* [35]*c*
7	E(N3) = −250 E(N2) = −80	900	10^4 $\mu m^{1}\cdot s^{-1}$	pH = 7	[90]*a* [33, 34]*c*
8		0.1 μM^{-1}	10*f* $\mu M^{-1}\cdot s^{-1}$		
9	E(N2) = −80 $E(CI.Q/CI.Q^{\cdot-})$ = −213*f*	0.005*f*	$4\cdot10^5$ $\mu M^{1}\cdot s^{-1}$	pH = 7	[90]*a*[35]*c*
The second electron transfer					
10	$E(FMN/FMNH^{\cdot})$ = −387 E(N1a) = −370	2	$2\cdot10^6$ $\mu M^{1}\cdot s^{-1}$	pH = 7	[89]*a* [35]*c*
11	$E(FMN/FMNH^{\cdot})$ = −387 E(N3) = −250	240	10^9 $\mu M^{-1}\cdot s^{-1}$	pH = 7	[89]*a* [35]*c*
12	E(N3) = −250 E(N2) = −80	900	10^4 $\mu m1\cdot s^{-1}$		
13		$2\cdot10^{13}$*f*	$2.7\cdot10^6$ $\mu M^{-1}\cdot s^{1}$	pH = 7	[35]*c*
14		20*f* μM	1000*f* s^{-1}		
NAD^+ reduction to NADH in mitochondrial matrix					
15		4.5	0.45 s^{-1}		[26]bc
Superoxide anion ($O_{2m}^{\cdot-}$) production by Complex I into the mitochondrial matrix					

Reaction No	Midpoint potential E_m=E, (mV)	Equilibrium constant K_{eq}	$k_{forward}$	Other parameters	Reference
16	$E(O_2/O_2^{\cdot-})$=−160 $E(FMNH^{\cdot}/FMNH^{-})$ = −293	204	2^f $\mu M^{-1}\cdot s^{-1}$	pH = 7	[62]^a
17	$E(Q/Q^{\cdot-})$ = −213^f $E(O_2/O_2^{\cdot-})$= −160	8.3^f	0.04^f $\mu M^{-1}\cdot s^{-1}$		[62]^a
Superoxide anion dismutation catalyzed by MnSOD in the mitochondrial matrix					
18				V_{max18} = 5.6 · 10^{4e} K_{m18} = 50 μM	[91] [92]
Succinate dehydrogenase reaction (Complex II)					
19				K_{19} = 0.6; V_{max19} = 256 mM/min (4270 μM/s)	[88]
Q and QH2 transmembrane diffusion					
20		1	22000 s^{-1}		[21]^c
21		1	22000 s^{-1}		[21]^c
Q_o–site reactions (Complex III)					
22		10^{-5} ^{f} μM^{-2}	0.1^f $\mu M^{-2}\cdot s^{-1}$		
23	ΔEm = −200 mV for the reaction	$3.4\cdot10^{-4}$	10^3 s^{-1}	pHo = 7.0 δ_1 = 0.2	[8]^{abc}
24		55^f μM	10^5 ^{f} s^{-1}		
25		40	10^5 ^{f} μM^{-1} s^{-1}	δ_2 = 0.5	[93]^b
26		10^{6f} μM	10^5 ^{f} s^{-1}		
27	E(ISPH) = 300 $E(c_1)$ = 270	0.3	10^5 ^{f} μM^{-1} s^{-1}	pHo = 7.0	[8]^{abc}
Superoxide anion ($O_2^{\cdot-}{}_{IMS}$) production by Complex III into the intermembrane space (IMS)					
28	$E(b_L.Q.ISPH/\ b_L.Q^{\cdot-}ISPH)$ = −160 $E(O_2/O_2^{\cdot-})$ = −160	1	2 $\mu M^{-1}\cdot s^{-1}$		[21]^a
Superoxide anion ($O_2^{\cdot-}{}_{mx}$) production by Complex III into the mitochondrial matrix					
29	$E(b_L.Q.ISPH/b_L.Q^{\cdot-}ISPH)$ = −160 $E(O_2/O_2^{\cdot-})$ = −160	1	2 $\mu M^{-1}\cdot s^{-1}$		[21]^a

Reaction No	Midpoint potential E_m=E, (mV)	Equilibrium constant K_{eq}	$k_{forward}$	Other parameters	Reference
Superoxide anion spontaneous dismutation and oxidation by cyt c in the intermembrane space (IMS)					
30			0.6 $\mu M^{-1}\cdot s^{-1}$	pHo = 7.0	[95]*c*
31	$E(O_2/O_2^{-}) = -160$ E(c) = 263	2.2·107	0.26 $\mu M^{-1}\cdot s^{-1}$		[62]*a* [96, 97]*c*
Q_i–site reactions (Complex III)					
32		0.022 μM^{-1}	2 $\mu M^{-1}\cdot \mu s^{-1}$		[98]bc
33		55	$5\cdot 10^4$ s^{-1}	pHi = 7.5 $\delta_3 = 0.3$	
34		40	$10^5 f$ s^{-1}	$\delta_2 = 0.5$	
35		0.67	$10^5 f$ s^{-1}	pHi = 7.5	
				$\delta_3 = 0.3$	
36		45 μM	$270f$ s^{-1}		[98]*b*
Cytochrome c reduction					
37		1.17	$2\cdot 10^3$ $\mu M^{-1}\cdot s^{-1}$		[99, 100]bc
38	$E(c_1) = 270$ E(c) = 263	0.8	$1.4\cdot 10^4$ s^{-1}		[94]*a* [99, 100]*c*
39		0.85	1.710^3 s^{-1}		[99, 100]bc
Cytochrome c oxidase reaction (Complex IV)					
40			$100f$ s^{-1}	$[O_2] = 2$ μM $k_{O2} = 1$ μM; $\Delta G^0 = -122.94$ kJ·mol^{-1}; pHi = 7.5 pHo = 7.0	[26, 101]

*a*Reference for the midpoint redox potential E_m

*b*Reference for the equilibrium constant K_{eq}

*c*Reference for the forward rate constant $k_{forward}$

*d*Value used is computed from the relation $K_{eq1} \cdot K_{eq2} \cdot K_{eq3} = \exp(2 \cdot F \cdot (E_{FMN} - E_{NAD+})/R \cdot T)$ in accord with the thermodynamic cycle pointed out by Kussmaul and Hirst [28], where midpoint redox potentials $E_{FMN} = -380$ mV (pH 7.0) and $E_{NAD+} = -320$ mV (pH 7.0), respectively, [32] and F, R and T have usual meaning.

[e] Value used is calculated from experimental data on Mn-SOD activity which is around of 8 U/mg mit. prot. = 8000 nmol/ min/mg mit. prot. [91]. So, V_{max18} normalized by the matrix volume is calculated in accord with the following equation (see Section 2.2 for detail): V_{max18} = Mn-SOD activity · 275 μM /60 s/Wmx = $5.6 \cdot 10^4$ μM/s.

[f] Values adjusted to match experimental data on kinetics of superoxide production.

Conserved moieties (nmol/mg mitochondrial protein): Complex I content which changes in different tissues from 0.1 to 0.4 [102, 103] was taken as 0.2 nmol/mg mit.prot, values of total ubiquinone and Complex III content were taken as follows [12], [total Q] = 4 nmol/mg mit.prot, [total cyt b_L] = [total cyt bH]= [total cyt c_1]= [total ISP]=0.325 nmol/mg mit.prot, and [total cyt *c*]=700 μM [49]. Translation of whole membrane concentration expressed in nmol/mg mit.prot. to local protein concentration expressed in μM presented in Section 2.2. Therefore, total local concentration of intramembrane proteins have the following approximate values expressed in μM: total Q = 4 nmol/ mg mit prot = 4541 μM; ISP = cyt b_L= cyt b_H= cyt c_1=0.325 nmol/ mg mit prot = 369 μM; FMN=N3=N1a=N2=0.2 nmol/ mg mit prot = 227 μM. The total concentration of NADH was taken 3000 μM [25].

Table 3

ROS production rates at different sites of ETC under varying respiratory substrate and inhibitor conditions in model L.

Inhibitor	Inhibited reaction rate in model L (Fig. 2A)	NADH			Succ			NADH + Succ		
		FMNH	CI.$Q^{\cdot-}$	b_L.$Q^{\cdot-}$ .ISPH	FMNH	CI.Q^{-}	b_L.Q^{-} .ISPH	FMNH	CI.$Q^{\cdot-}$	b_L.$Q^{\cdot-}$ .ISPH
None		+++ 3A	+ 3B	++ 3C	≈0 3A	+++ 3B	+ 3C	+++ 3A	+ 3B	+++ 3C
Rotenone	$v_8 = 0$ $v_{14} = 0$	+++ 3A	−−− NSh	−−− NSh	−−− Expct	−−− Expct	0 Expct	+++ Expct	−−− Expct	− Expct
Antimycin A	$v_{34} = 0$	+++NSh	0 NSh	+++ NSh	+++ NSh	−−− NSh	+++ 5D	+++ Expct	−−− Expct	+++ Expct
Myxothiazol	$v_{24} = 0$	+++ NSh	0 NSh	+++ NSh	+++7B	−−− 7C	+++ 7D	+++ Expct	−−− Expct	+++ Expct
Stigmatellin	$v_{23} = 0$	+++ NSh	0 NSh	−−− NSh	+++ 7B	−−− 7C	−−− 7D	+++ Expct	−−− Expct	−−− Expct
Azide, KCN	$v_{40} = 0$	+++ 8B	0 8C	−− 8D	+++ 9B	−−− 9C	−− 9D	+++ Expct	−−− Expct	−− Expct
Cyt *c* depletion		+++ 10B	0 10C	−− 10D	+++ 11B	−−− 11C	+/− 11D	+++ Expct	−−− Expct	−− Expct
IMM depolarization		−− 3A	−− 3B	+/− 3C	−− 3A	−−− 3B	+/− 3C	−− 3A	−− 3B	+/− 3C

* Symbols +, ++, +++ and −, −−, −−− indicate low, intermediate, or large increase or decrease in ROS production rate, respectively, compared to ROS production rates under uninhibited condition, or, for the uninhibited condition, the change in ROS production rate upon addition of respiratory substrate.

** Symbol +/− indicates variable effect depending on membrane potential.

*** NSh, computed but not shown; Expct, not computed but expected results.

**** 3A-11D refers to the relevant Figures in the text.